INDIAN INSTITUTE OF TECHNOLOGY MADRAS

DSP System Analysis for Linear and Nonlinear Impairments in Optical Communication Systems

by

Aditya Sant

EE12B071

A thesis submitted in partial fulfillment for the
BACHELOR OF TECHNOLOGY & MASTER OF TECHNOLOGY

in the
Department of Electrical Engineering

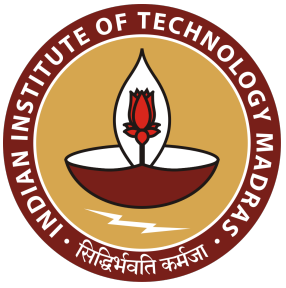

June 2017

THESIS CERTIFICATE

This is to certify that the thesis titled **DSP System Analysis for Linear and Non-linear Impairments in Optical Communication Systems**, submitted by **Aditya Sant**, to the Indian Institute of Technology, Madras, for the award of the degree of **BACHELOR OF TECHNOLOGY & MASTER OF TECHNOLOGY**, is a bona fide record of the research work done by him under our supervision. The contents of this thesis, in full or in parts, have not been submitted to any other Institute or University for the award of any degree or diploma.

Prof. Deepa Venkitesh
Dual-degree Guide
Associate Professor
Dept. of Electrical Engineering
IIT-Madras, 600 036

Prof. David Koilpillai
Dual-degree Co-Guide
Professor
Dept. of Electrical Engineering
IIT-Madras, 600 036

Place: Chennai

Date: 2nd June 2017

INDIAN INSTITUTE OF TECHNOLOGY MADRAS

Abstract

Department of Electrical Engineering

Bachelor of Technology & Master of Technology

by Aditya Sant
EE12B071

This report is divided into 2 main parts for each project. The common link is the use of DSP for compensation of impairments for optical communication, albeit in two distinct scenerios.

The first 4 chapters analyze the impairments in the domain of high-speed, coherent optical communication. The specific impairment of phase noise is discussed in detail and the approach of Kalman Filtering for this compensation is presented.

The second half of this report presents the work done in the paradigm of underwater optical communications. A novel technique, using Second Harmonic Generation is used for transmission in this medium. The specific nonlinear impairments associated with this are brought to light. Implementation of spectrally efficient modulation: OFDM, is analyzed in this context, keeping the benchmark of the presently implemented system: PPM (Pulse Position Modulation)

Acknowledgements

I would like to begin by thanking my guide, Prof. Deepa Venkitesh for all her help, support and patience throughout the course of my project work. Her approach and dedication to research has been incomparable and has always inspired me to keep pushing myself. I also extend my heartfelt gratitude to Prof. David Koilpillai for all the helpful discussion and inputs on the project. I would also like to give a huge thank you to the entire Photonics Research Group at IIT Madras for all the help, resources and guidance throughout my research work. All the PhD and Masters students in the OCEAN Lab have been immensely cooperative, friendly and accommodating and have greatly inspired my own work. I would like to put in a special thank you to Prof. Balaji Srinivasan, whose "Introduction to Photonics" course motivated me to explore the subject of optical communication.

Were it not for the infallible faith of my parents and brother, I would not be present here. They have been a constant support throughout my life and I am forever grateful to them for their blessing and encouragement..

Lastly, I would like to give a huge shout-out to every one of my friends who have made the experience at IIT Madras, a treasured one. A special thank you to Bhavik, Deshmukh, Bhadane, Kaustubh, Deokule, Adit and Avni for countless memories and experiences, that will stay with me forever.

Contents

List of Figures

List of Tables

Abbreviations

DSP	**D**igital **S**ignal **P**rocessing
PN	**P**hase **N**oise
FM	**F**requency **M**odulation
KF	**K**alman **F**ilter
EKF	**E**xtended **K**alman **F**ilter
CD	**C**hromatic **D**ispersion
LO	**L**ocal **O**scillator
FO	**F**requency **O**ffset
PMF	**P**olarization **M**aintaining **F**iber
PDM	**P**olarization **D**ivision **M**ultiplexed
ADC	**A**nalog to **D**igital **C**onverter
DDLMS	**D**ecision-**D**irected **L**east **M**ean **S**quare
SNR	**S**ignal to **N**oise **R**atio
OSNR	**O**ptical **S**ignal to **N**oise **R**atio
BER	**B**it **E**rror **R**ate
QPSK	**Q**uadrature **P**hase **S**hift **K**eying
QAM	**Q**uadrature **A**mplitude **M**odulation
AWG	**A**rbitrary **W**aveform **G**enerator
OFDM	**O**rthogonal **F**requency **D**ivision **M**ultiplexing
PPM	**P**ulse **P**osition **M**odulation
SHG	**S**econd **H**armonic **G**eneration
IM	**I**ntensity **M**odulation
EDFA	**E**rbium **D**oped **F**iber **A**mplifier
USRP	**U**niversal **S**oftware **R**adio **P**eripheral

Physical Constants

Speed of Light	c	$=$	$3 \times 10^{8} ms^{-1}$
Plank's Constant	h	$=$	$6.62 \times 10^{-34} Js$
Permittivity of free space	ϵ_0	$=$	$8.85 \times 10^{-12} m^{-3} kg^{-1} s^{4} A^{2}$
Permiability of free space	μ_0	$=$	$1.25 \times 10^{-6} mkgs^{-2} A^{-2}$

Symbols

$\vec{E}$	Electric field	V/m
$\vec{P}$	Electric polarization	Asm^{-2}
P	Power	W (Js^{-1})
f	Optical/Electrical frequency	Hz
λ	Optical wavelength	m
ω	angular frequency	$rads^{-1}$
n^{ω}	Modal Refractive index at ω	
k	Propagation constant	m^{-1}
Δk	difference between propagation constants	m^{-1}
α	Constant in SHG equation	

Chapter 1

DSP for High Speed Coherent Optical Communication: Phase Noise

This chapter introduces one of the major impairments in coherent optical communication: Laser Phase Noise. The reason for the effect of phase noise is clearly stated, more importantly, the consequences for optical communication. The analysis of the laser phase noise is presented in both the time domain as well as the frequency domain. Two distinct methods for phase noise generation are elaborated with the given characteristics described. Subsequent chapters go on to deal with a specific algorithm to counter this phase noise, particularly using the properties of the noise discussed.

1.1 Introduction

Coherent Communication using fiber optic technologies involves the manipulation of the different parameters of the optical field.

$$\vec{E}(t) = E_0(t)exp(\omega t - \beta z + \phi(t))\hat{p} \tag{1.1}$$

As can be seen from the above equation, coherent communication involves modulation of the optical field intensity, phase as well as the polarization. However, recovery of the information from the optical signal, requires a DSP block in the receiver architecture.

High speed coherent communication systems have a huge dependence on the DSP back-end for compensation of different impairments with transmission of data. Today, advanced DSP algorithms are used to combat the impairments related to Polarization Mode Dispersion, Frequency Offset, Chromatic Dispersion, Timing Recovery, Phase Noise Compensation and IQ Balancing. Using advanced DSP techniques, high data rates through spectrally efficient modulation formats can be achieved. DSP compensation has been widely applied to wireless communication systems to reach higher, noise tolerant data rates. However, through the next few chapters, this report focuses mainly on the impairment and compensation of the data through the Laser Phase Noise. The next secion provides an overview of the laser phase noise. The spectral properties of this noise are then expressed in detail and then, a linear model to simulate the laser phase noise is explained.

1.2 Phase Noise in Coherent Communication

Any real laser has random fluctuations in amplitude and phase. These are caused due to the spontaneous emission in the crystal, adding power to the optical field. This added power causes a deviation from the existing monochromatic field, resulting in the spectral broadening of the laser field, creating a laser linewidth. This is illustrated below.

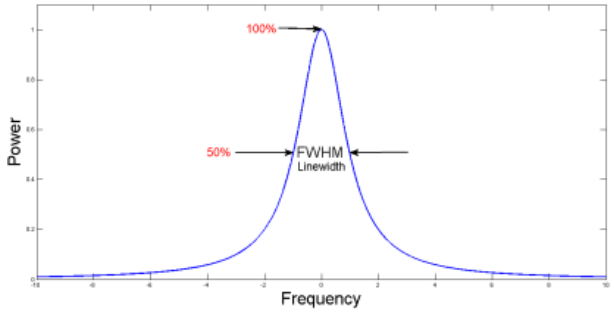

FIGURE 1.1: Spectral Broadening of the Laser Field

The modulated electric field in lasers is given as:

$$E(t) = \sqrt{P(t)}exp(j\omega_c(t) + \phi_m(t) + \phi(t)) \tag{1.2}$$

Here, $P(t)$ represents the input power. In the case of amplitude modulation, this is varied as a function of time. The term $\phi_m(t)$ is the phase modulation, if it is present in the system.

The term $\phi(t)$ represents the phase noise in the system. It is a random variable, given as a function of the laser linewidth. Such phase noise counts as a critical impairment for phase modulation and coherent detection.

As can be seen in Figure(1.1), the Power Spectral Density(PSD) of the laser has a Lorenzian lineshape [1]. The linewidth Δf, of this spectrum is a measure of the variance of the phase noise.

Let the transmitted symbol duration be T.

$$\Delta\phi_T(t) = \phi(t) - \phi(t - T) \tag{1.3}$$

The phase error variance within this interval is given as:

$$\sigma_\phi^2(T) = \langle \Delta\phi_T(t)^2 \rangle \tag{1.4}$$

If the noise samples have no correlation among them, the variance is a linear function of the linewidth,

$$\sigma_\phi^2(T) = 2\pi\Delta fT \tag{1.5}$$

However, this linear model of the phase error variance is not valid for all cases. The phase noise values are not uncorrelated in the time domain, as is the case of AWGN, but have a correlation between samples. This is further expalined in the following section.

1.3 Spectral Properties

In the previous section, it was shown that for a uniform $AWGN$ noise, the noise variance is a linear function of the correlation interval T.

However, phase noise noise has a very prominent time domain correlation, translating to a spectral shaping of the frequency, for lower frequency values. Delayed Self-Heterodyne measurements with DFB and SGDBR lasers, have demonstrated this spectral dependence of the noise [2].

The FM noise spectrum is defined as the PSD of the instantaneous frequency, got by differentiating the phase noise. The analytical spectrum is given as [3]:

$$S_f(f) = S_0 + \frac{K_1}{f} + \frac{K_2}{f^2} = S_0\left[1 + \frac{f_1}{f} + \frac{f_2}{f^2}\right] \tag{1.6}$$

The specific $1/f$ noise term is known as flicker noise and the $1/f^2$ term is known as random-walk noise.

In addition, S_0 is PSD of the uniform white noise, f_1 and f_2 are the corner frequencies of the flicker noise and the random noise, respectively.

The following plot shows the noise spectrum.

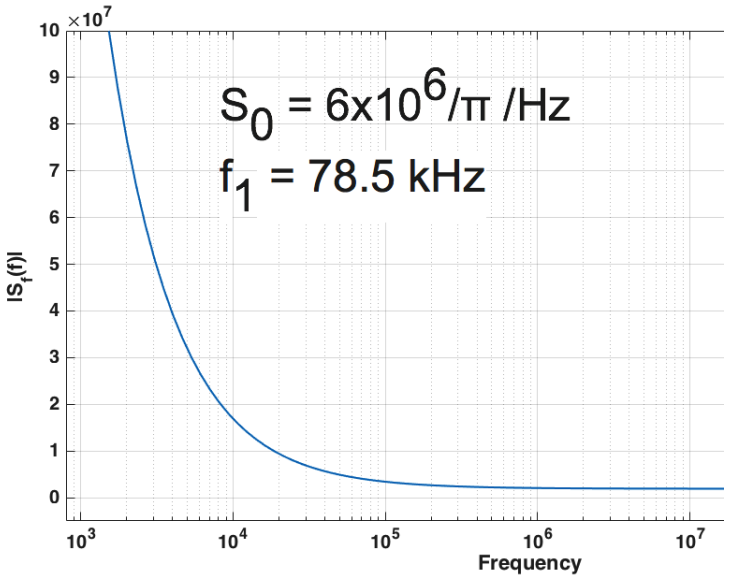

FIGURE 1.2: Theoretical FM Noise Spectrum

Using the analytical spectrum, the phase error variance is expressed as:

$$\sigma_\phi^2(T) = 4\int_{f_l}^{f_u} S_f(f)\frac{sin^2(\pi f T)}{f^2}df \tag{1.7}$$

On performing these integrations, the phase error variance is given as,

$$\sigma_\phi^2(T) = 2\pi\Delta f T\Big\{1 + [1.5 + Ci(2\pi f_u T) - Ci(2\pi f_l T)]2f_1 T\Big\} \tag{1.8}$$

- "$Ci(x)$" is the cosine integral, given as $Ci(x) = -\int_x^\infty [cos(t)/t]dt$
- The FM noise yields linear phase-error variance over short symbol duration, but deviates from linearity over longer symbol duration; thus the flicker noise affects low baud rate systems
- An important assumption considered here is that, since the random-walk cutoff frequency f_2, occurs well below the flicker noise frequency f_1, the effect of this noise is felt at much lower data rates; hence the contribution of this term to the phase variance is neglected

1.4 Phase Noise Generation: Simulation of Phase noise

This section presents a method for generation of flicker noise, using input as the laser linewidth and the baud rate. For the low baud rate systems considered, we consider the only the flicker noise. The white noise is not taken, and the analysis is done, considering the strong correlation and the $1/f$, dependence of the noise.

1.4.1 Linear noise model

For simulation of phase noise with the $\frac{1}{f}$ characteristic, the general theory of modeling $\frac{1}{f^\alpha}$ noises is used.
The linear model of noise is given as the convolution of a fixed LTI system with a white noise system. [4]

$$x(t) = \int_0^t h(\beta)w(t-\beta)d\beta \tag{1.9}$$

Here, $h(t)$ is the impulse response of the linear system and $w(t)$ is the white noise. In order to model the impulse response h(t), for the 1/f noise, the statistical model of Fractional Brownian Motion is used. The white noise is given as the fractional derivative of the 1/f noise. The anti-derivative is calculated through the Reimann-Liouville integral, as shown by the equations below.

$$\frac{d^\alpha x(t)}{dt^\alpha} = w(t) \tag{1.10}$$

$$x(t) = \frac{1}{\Gamma(\alpha/2)} \int_0^t (t-\tau)^{\frac{\alpha}{2}-1} w(\tau) d\tau \tag{1.11}$$

Based on this, we can use the linear model in eq (3) , described above to define the impulse response h(t) as:

$$h(t) = \frac{t^{\frac{\alpha}{2}-1}}{\Gamma(\alpha/2)} \tag{1.12}$$

1.4.2 Discrete time noise generation

For simulation in discrete time, we use the properties of this linear noise model in the discrete time domain.
In discrete time, the z-transform is presented as the generalization of the random walk process.

$$H_f(z) = \frac{1}{(1-z^{-1})^{\alpha/2}} \tag{1.13}$$

The values of the coefficients for H(z) are computed as:

$$h[k] = \frac{\Gamma(\alpha/2+k)}{k!\Gamma(\alpha/2)} \tag{1.14}$$

Mathematically, this is a closed for expression for a series of coefficients which can e computed iteratively.

$$h[0] = 1 \tag{1.15}$$

$$h[k] = (\frac{\alpha}{2} + k - 1)\frac{h[k-1]}{k} \tag{1.16}$$

Through the equations above, we generate the impulse response $h(t)$. Convolution of this impulse response with the white Gaussian noise gives flicker noise with a decaying $\frac{1}{f}$ nature. In order to simulate the exact nature of the noise, this is further shifted up, by adding white Gaussian noise to the flicker noise. Thus we are able to generate the frequency spectrum as predicted by the analytical model as well as observed by the self-heterodyne measurement. However, we only simulate the flicker noise.

$$x(t) = h(t) * w_1(t) \tag{1.17}$$

Here, ' * ' denotes the convolution operation and w_1 is an independently generated white Gaussian noise process.

The output $x(t)$ is array, which consists of the extra phase that is to be added to the laser electric field.

The following is the plot for the noise spectrum for the simulated noise, described above.

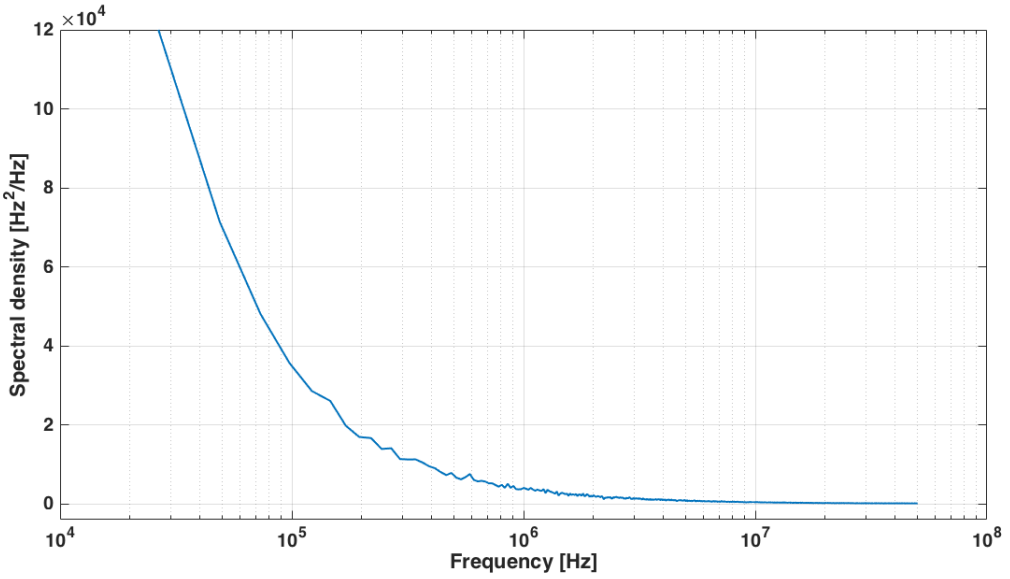

FIGURE 1.3: Simulated FM Noise Spectrum

- This above method is an illustrative analysis to show that this linear system approach can produce phase noise samples with the $1/f$ characteristics
- Although the following plot does not correspond exactly to the ideal plot above, in terms of the corner frequencies and the white noise PSD, it has the same characteristic behavior
- The exact spectral properties and the corner frequencies can be achieved by adjusting the parameters of the white noise variance for convolution with the linear filter in the discrete noise generation model

1.5 Extent of Analysis Done

The analysis done with respect to the phase noise is presented below.

- A specific compensation algorithm for phase noise tracking is analyzed: Kalman Filtering
- The optical communication chain is simulated and the different impairments are added; compensation of the different impairments are done through standard established algorithms, mentioned later
- Experimental validation of the KF algorithm is presented, comparing it with DD-LMS for phase noise correction
- An Extended Kalman Filter(EKF) approach to combined phase noise tracking and polarization state tracking is also presented and analyzed in the subsequent chapters

Chapter 2

KF: Phase Noise Tracking Algorithm

This chapter introduces the Kalman Filter(KF) algorithm to track the phase noise of the laser and compensate it. It introduces the mathematical construct of the KF equations for any general model. These equations are then specifically modified to track laser phase noise. The chapter goes on to discuss the performance, as well as the limitations of the algorithm. The validity

2.1 KF Equations

The KF is based on a state-space model of linear dynamic systems. It is a single tap optimal filtering technique that recursively estimates the parameter to be analyzed. It uses the noise properties of the generation as well as the measurement of the variable to adapt its gain coefficient for estimation. One of the key advantages of the algorithm is in terms of its memory usage; KF only uses the previous estimate to generate each new value of the same, and hence is not very memory intensive.

2.1.1 System parameters

The minimal set of data that is sufficient to uniquely describe the unforced, dynamical behavior of the system, is known as the state: $x(k)$. This state is transformed over

time. It is a function of the current value of the state, the input, $u(k)$, and is subject to process noise.
The state equation is given as follows.

$$x(k+1) = F(k)x(k) + G(k)u(k) + v(k) \tag{2.1}$$

Here, v(k) is the process noise.

The state cannot be observed directly. In order to observe the state, it undergoes a transformation, known as the measurement. This measurement is subject to measurement noise which also corrupts the measurement.
The measurement equation is given as follows.

$$z(k+1) = H(k)x(k) + w(k) \tag{2.2}$$

Here, w(k) is the measurement noise.

The convention $x(k|k)$ is used to denote that the value of $x(k)$ is a function of all the values before it. In addition, the quantity $P(k)$ is the state covariance, which is a matrix in the generalized case. The state covariance matrix describes the effect of the time steps on the cavariances of errors in estimation of the state. Initially, we are given the knowledge of $\hat{x}(k|k)$, $P(k|k)$ and $u(k)$. The new measurement is given by $z(k+1)$.

2.1.2 KF equations

The KF process is a linear estimation of the state $x(k)$, using the information contained in the observation $y(k)$, given the prior estimate of this same state. The detailed approach to arrive at the final KF equations can be found in different texts.[5] However, here the final equations are presented. The generalized KF equations are given by the following. [6]

1. State estimation

- State prediction

$$\hat{x}(k+1|k) = F(k)\hat{x}(k|k) + G(k)u(k) \tag{2.3}$$

- Measurement prediction

$$\hat{z}(k+1|k) = H(k)\hat{x}(k+1|k) \tag{2.4}$$

- Measurement residual

$$v(k+1) = z(k+1) - \hat{z}(k+1|k) \tag{2.5}$$

- Updated state estimate

$$\hat{x}(k+1|k+1) = \hat{x}(k+1|k) + W(k+1)v(k+1) \tag{2.6}$$

  Here $W(k+1)$ is the Kalman gain, as is shown in the state covariance estimation

2. State covariance estimation

- State prediction covariance

$$P(k+1|k) = F(k)P(k|k)F(k)' + Q(k+1) \tag{2.7}$$

  $Q(k+1)$ is process noise covariance matrix

- Measurement prediction covariance

$$S(k+1) = H(k)P(k+1|k)H(k)' + R(k+1) \tag{2.8}$$

  $R(k+1)$ is measurement noise covariance matrix

- Filter gain

$$W(k+1) = P(k+1|k)H(k+1)'S(k+1)^{-1} \tag{2.9}$$

- Updated state covariance

$$P(k+1|k+1) = P(k+1|k) - W(k+1)S(k+1)W(k+1)' \tag{2.10}$$

2.2 KF Equations for Phase Noise

A specific application of these generalized equations is used to track the phase noise of the system. The advantage of the KF approach is that is takes into account the generation model of the noise. The compensation of such an impairment is thus robust to the system noise present. The model is used for phase noise tracking as follows: [7]

- The state variable is the phase ψ_k
- The measured value is z_k
- Received signal after CD and FO compensation is given as $r_k = s_k exp(j\psi_k) + n_k$
- ψ_k is the phase noise term for the k^{th} received symbol

2.2.1 Phase noise model used

The phase noise ψ_k is generated as a Weiner process.

$$\psi_k = \psi_{k-1} + \delta_k \tag{2.11}$$

Where, δ_k is a zero mean Gaussian random variable with variance as a function of the laser linewidth.

2.2.2 KF equations for phase noise tracking

The measurement variable z_k is calculated as follows.

$$z_k = \angle(r_k s_k^*) \qquad = \psi_k + \tilde{n}_k \tag{2.12}$$

The Kalman gain is given by K_k, the state covariance for the symbol is given as σ_k^2, the process noise covariance is Q and the measurement noise covariance is R.

The equations for the phase noise tracking are given as follows.

$$\hat{\psi}_{k+1} = \psi_k + K_k(z_k - \hat{\psi}_k) \tag{2.13}$$

$$\sigma^2_{k+1} = \frac{\sigma^2_{k+1}R}{R + \sigma^2_{k+1}} + Q \tag{2.14}$$

$$K_k = \frac{\sigma^2_{k+1}R}{R + \sigma^2_{k+1}} \tag{2.15}$$

2.3 Algorithm Performance

This section provides an analysis of the algorithm performance. The metric to measure this performance is the Bit Error Rate (BER) of the received signal, as a function of the different Optical Signal to Noise Ratio (OSNR) values.

2.3.1 Implementing the KF algorithm

The previous equations were used to implement phase noise tracking. One of the main advantages over the Decision Directed - Least Mean Square (DD-LMS) approach was that the KF was implemented as a purely **blind algorithm**. There is no need to know the training sequence. The following are some the comments on the implementation of the algorithm.

- The convergence for the training mode, depends on the convergence of the gain(K_k) and the state covariance($\sigma^2{}_k$)
- The update equations for both K_k and $\sigma^2{}_k$ are independent of the estimate for the phase noise or the difference from the actual value
- Hence, to make the algorithm blind, a pseudo-training sequence is taken to make the KF achieve convergence
- The length of the pseudo-training sequence depends on the total number of symbol samples; for the simulation of BER Vs OSNR: the same, 64 length sequence was taken

- For the first 64 received samples the pseudo training sequence was taken as the ideal constellation point, using the nearest neighbour rule
- After the value of the gain converges, the phase estimation is restarted from the first sample
- As explained earlier, since the convergence is independent of the accuracy of the estimate, this approach performs the same as one with a known training sequence

2.3.2 OSNR generation

In addition to the phase noise present, the following other noise sources are considered.

- Laser ASE noise, taken as $30dB$ below the transmit power
- Noise added by the optical amplifier with a given noise figure

In order to simulate varying OSNR conditions, the noise figure of the EDFA is varied as a function of the desired OSNR.
For the EDFA, the noise figure is given by:

$$F_n = \frac{(SNR)_{in}}{(SNR)_{out}} \tag{2.16}$$

$$(SNR)_{in} = \frac{P_{in}}{2h\nu\Delta f} \tag{2.17}$$

Here Δf corresponds to a linewidth of $0.3nm$. For high gain, $F_n = 2n_{sp}$, where n_{sp} is the spontaneous emission factor, given as a function of the wavelength, transmit power, symbol rate and desired output OSNR.
By varying the value of the output OSNR, we vary the range of the amplifier noise figure F_n

2.3.3 Choice of parameters: Q and R

Since the noise model is taken as a Weiner Process, for the generation for the phase noise. The optimal values for Q(process noise covariance) and R(measurement noise cavariance) are chosen as: [8]

- $Q = \frac{2*\pi*\Delta\lambda}{R_{symb}}$
  $\Delta\lambda$ is the laser linewidth and R_{symb} is the symbol rate
- $R = \frac{1}{2*OSNR}$

2.3.4 Simulation and performance analysis

The algorithm was tested for both QPSK and 16QAM constellations and hence, and compared to the theoretical limit for both these constellations in terms of the OSNR.

- QPSK: $BER = \frac{1}{2}erfc(\sqrt{\frac{OSNR}{2}})$
- 16QAM: $BER = \frac{3}{8}erfc(\sqrt{\frac{OSNR}{10}})$

The parameters for the simulation was as follows:

- The baud rate was taken as $25Gbaud$
- The laser linewidth was varied and the performance was analyzed as function of the phase error variance
- The OSNR was varied from 5 to 30 dB
- The number of symbols taken was limited to 2^{12}
- In order to test KF performance strictly, there were no other impairments added

The figure (2.1) shows the OSNR Vs BER plots for both the QPSK and thr 16QAM constellation.

- As can be seen from the plots the performance is limited by the laser linewidth
- However, the tracking is independent of linewidth, provided that there is no cycle-slip; this is separately elaborated in the next section
- For linewidths in the range of MHz, the phase noise takes a large angular spread, and hence there are different challenges to track this phase
- With respect to, cycle slip as well, the 16QAM constellation is much more susceptible to large noise spread as compared to the QPSK; this is expected intuitively as well

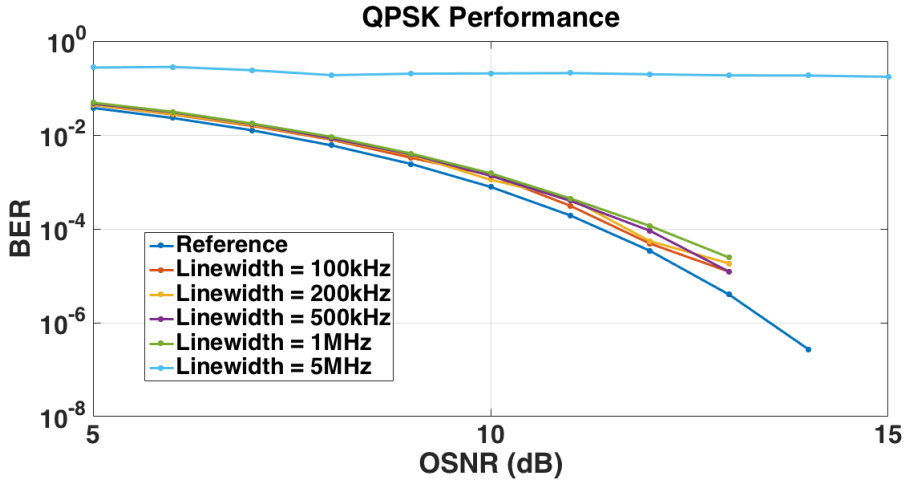

(a)

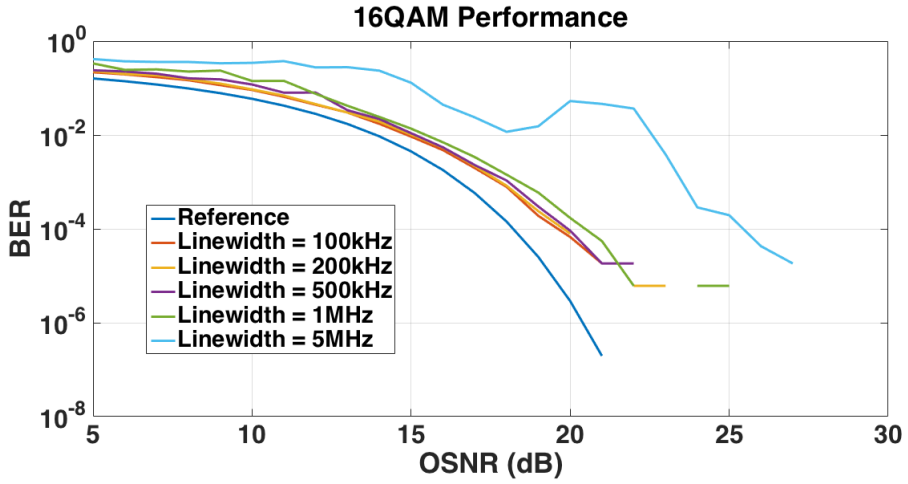

(b)

FIGURE 2.1: Performance of KF for Different Constellations

2.4 Limitations

- One of the major limitations of the simulation is in terms of the number of symbols: this results in the BER analysis to be accurate to an order of 10^{-5}
- The main reason for limiting the number of symbols is the cycle slip for phase estimation, this is further illustrated below

2.4.1 Simulation limitation: Number of symbols and phase noise

This section raises a specific point about the limitations while generating random numbers while simulation of the phase noise

- As is discussed in the above chapters and sections, the phase noise process is a random process
- The process of generating random numbers limits the total number of symbols taken in the simulation
  - If the number of symbols is large, the number of points with large amplitudes increases, for small values of variance
  - In the context of phase noise: if we take a large number of symbols, the spread of the constellation increases, even for small phase error variances(order of $100kHz$)
  - This statistical generation principle limits the total number of symbols to the order of 2^{14}
- For symbols acquiring a phase error greater than π, the KF algorithm incorrectly tracks the phase, resulting in a cycle slip, as explained in the next section

2.4.2 Cycle slip in phase estimation

Due to the large number of symbols taken, the phase error of the symbols has a larger spread. This causes some symbols to acquire a phase beyond $\pm\pi$.
The following plot illustrates the cycle slip present in phase estimation.

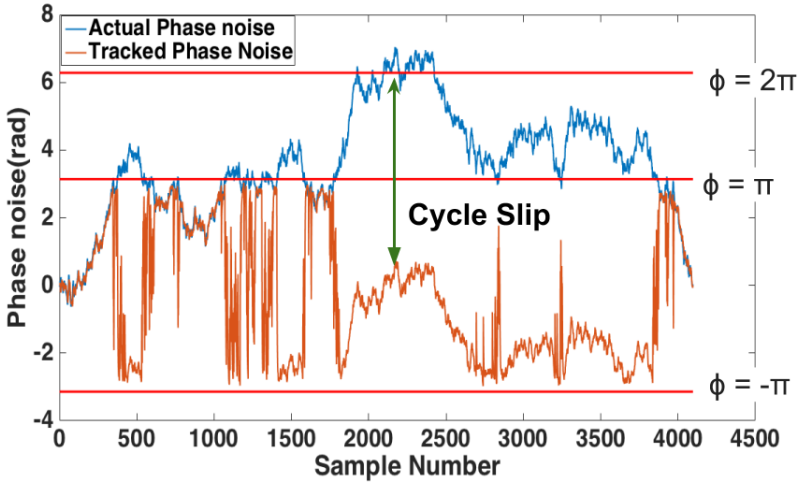

FIGURE 2.2: Illustration of cycle slip for large phase noise

- As can be seen in figure (2.2), the phase estimation fails when the actual phase error crosses the threshold of $[-\pi\ \pi]$
- To explain this, the algorithm is again analyzed: eq (2.12), i.e, the measurement equation for the KF calculates the angle of the complex number, which by definition, lies between $[-\pi\ \pi]$
- However, it is also noted that although there is a jump in the tracked phase noise, the tracking still follows the actual phase noise
- In order to compensate such a cycle slip, different approaches are used for wrapping the phase: however this is highly dependent on the OSNR present and hence aren't completely reliable
- Different unwrapping algorithms were experimented, however, they all fail at lower SNR values; hence this is concluded as a limitation of this algorithm
- For a cycle slip to occur, the phase noise should cross π, which is highly unlikely for all practical applications and hence the effect of the cycle slip is safely neglected

The next chapter goes on to extend the KF to compensate for polarization mixing as well as phase noise tracking as well.

Chapter 3

EKF for Combined Polarization State and Phase Noise Tracking

This chapter uses the Extended Kalman Filter(EKF) implementation to track both polarization state as well as phase noise.[9] The problem description for polarization state tracking is presented as an impairment. The EKF equations are then explained, which are used to track and compensate these impairments. Critical differences between the approach for phase noise tracking and EKF for combined tracking are also stressed. In addition to analyzing the performance and its limitations, an improvement in the algorithm is also presented, making it more robust.

3.1 Polarization Mixing: Problem Description

This section introduces the notion of polarization mixing and motivates and the system model to describe the changes.

3.1.1 Theoretical overview

Information in the light wave can be transmitted through various degrees of freedom. One of the main such degrees is using the polarization of the light. This implies that the data can be simultaneously transmitted on the 2 orthogonal polarizations, and hence be used to double the effective data rate.

Assuming that the 2 polarizations have equal amplitudes and the wave is transmitted along the $\hat{z}$ direction, the electric field can be mathematically written as:

$$\vec{E}(t) = E_0 e^{(j\omega t + \phi_x(t))}\hat{x} + E_0 e^{(j\omega t + \phi_y(t))}\hat{y} \tag{3.1}$$

Here, we have omitted the propagation, as it does not carry any phase information. Clearly, the terms $\phi_x(t)$ and $\phi_y(t)$ represent the 2 distinct modulations for each polarization.

For ease of illustration, we represent the vector as an array, consisting of the two distinct terms for the two orthogonal polarizations. This is further elaborated below.

3.1.2 Modeling the system

The original dual polarization constellation vector is represented as:

$$\begin{pmatrix} H \\ V \end{pmatrix}$$

The received vector, corrupted with noise is represented as:

$$\begin{pmatrix} X \\ Y \end{pmatrix}$$

Unless the fiber used is a polarization maintaining fiber (PMF), the two polarizations intermix among themselves. This mixing is modelled through a simple unitary transform, i.e, multiplication of the electric field vector by a unitary matrix. This matrix is known as the Jone's matrix. The Jone's matrix for the polarization mixing is J, and is in the form:

$$\begin{pmatrix} a - jb & -c - jd \\ c - jd & a + jb \end{pmatrix}$$

Since the matrix is unitary, we have the constraint: $a^2 + b^2 + c^2 + d^2 = 1$.

Since we are dealing with the combined compensation of the polarization mixing as well as the laser phase noise, we will further include the phase noise term multiplied by the two polarizations. A very important assumption made here is that, since the same

laser is used to polarize the samples in the $\hat{x}$ and $\hat{y}$ direction, the same magnitude of the phase noise is added to both the polarizations.
So the overall noise model for combined polarization mixing and phase noise is given as:

$$h_i = \begin{pmatrix} H \\ V \end{pmatrix} = e^{j\theta} \begin{pmatrix} a+jb & c+jd \\ -c+jd & a-jb \end{pmatrix} \begin{pmatrix} X \\ Y \end{pmatrix} \tag{3.2}$$

We write the form as the recovery of the uncorrupted data from the received signal. Here, the matrix above is verified to be the inverse Jones matrix.

3.2 EKF approach

This model for combined polarization mixing and the phase noise presents the starting point for applying Kalman Filtering for data recovery. Here, we cannot use the same KF applied for phase noise recovery, as there is a nonlinear phase term present. Thus, we use an EKF approach to recover the data. [9]

3.2.1 State and process variables

The following are the different variables taken:

- The state variable, S_i is taken as $\begin{pmatrix} a & b & c & d & \theta \end{pmatrix}'$
- The state error covariance, P_i is a 5×5 square matrix
- The compensated symbol vector is h_i and is the same 2×1 array as explained above
- The Jacobian for the system is M_i and is equal to

$$M_{jk|i} = \frac{\partial h_j}{\partial S_k} \tag{3.3}$$

Hence M_i is a 2×5 matrix given as:

$$M_i = e^{j\theta} \begin{pmatrix} X & jX & Y & jY & jaX - bX + jcY - dY \\ Y & -jY & -X & jX & -jcX - dX + jaY + bY \end{pmatrix} \tag{3.4}$$

- The Kalman gain is given as K_i
- The residual for the Kalman gain is calculated by taking the nearest constellation point Z_c
- The process and measurement noise covariances are given as Q and R respectively

3.2.2 EKF equations

The following are the Kalman filter equations

$$S_i^- = AS_{i-1} \tag{3.5}$$

$$P_i^- = AP_{i-1}A^T + Q \tag{3.6}$$

$$K_i = P_i^- M_i^T [M_i P_i^- M_i^T + R]^{-1} \tag{3.7}$$

$$S_i = S_i^- + K_i[Z_{ci} - h_i] \tag{3.8}$$

$$P_i = P_i^- - K_i M_i P_i^- \tag{3.9}$$

Since the phase noise is implemented as a random walk process, the value of the matrix A is the identity matrix. The matrix Q and R are still the process noise covariance and the measurement noise covariance, as explained in the earlier chapter.

The values to be estimated are real, whereas the EKF equations are complex valued. A small change to the equations is made to the equations $(3.5) - (3.9)$*, to overcome this. Whenever, the complex matrices* M_i*,* h_i *or* Z_{ci} *are generated, the complex rows are split into two: the real and imaginary parts. Accordingly the dimension of* K_i*,* Q *and* R *are appropriately chosen.*

3.3 Performance and Critical Limitations for EKF

The following section shows the performance of the EKF with simulated dual polarization data. More importantly, an important limitation of the algorithm is highlighted.

3.3.1 Implementation with simulated data

The following algorithm is simulated for both QPSK and 16QAM. The following shows the results. The constellation plots for the same are as given.

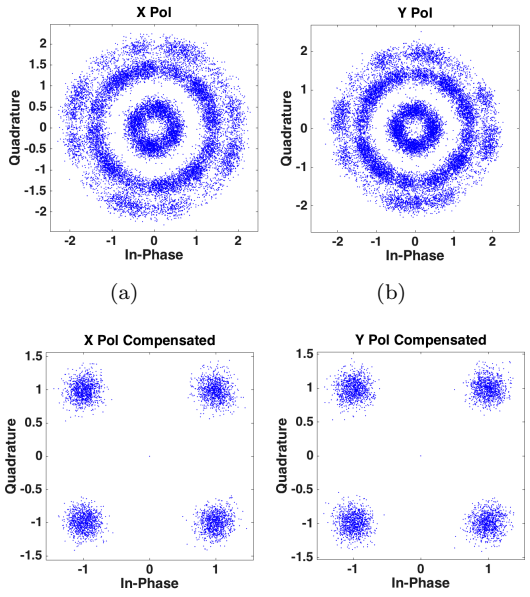

FIGURE 3.1: QPSK constellation

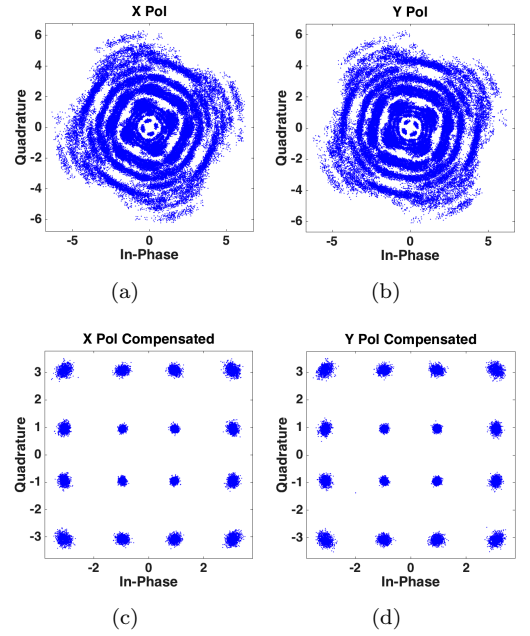

FIGURE 3.2: 16QAM constellation

3.3.2 EKF performance

The figure(3.3) shows the BER as a function of the OSNR for the QPSK constellation. The 16QAM performance also follows a similar plot.

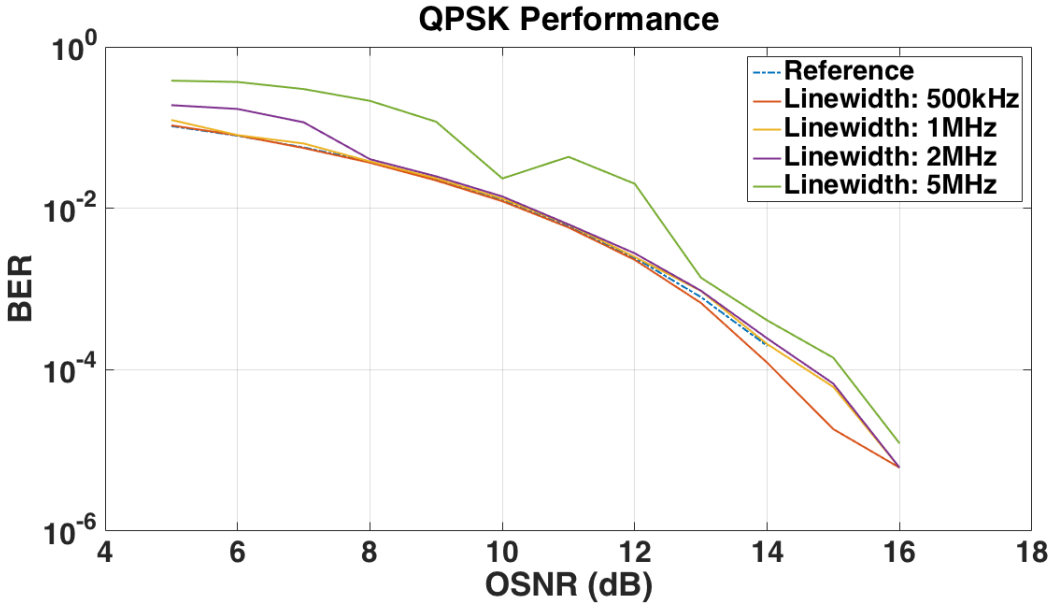

FIGURE 3.3: EKF Constellation Performance

- The performance of this algorithm is very close to the theoretical limit, indicating efficient convergence
- For larger linewidths, the cycle slip comes into consideration, which affects the performance of the phase tracking, as explained before
- However, this algorithm too has some limitations, which are further discussed below

3.3.3 EKF limitation

One of the major limitations of the EKF algorithm, is that it requires a training sequnce for convergence. In eq(3.8), the value of the residual, depends on the value of Z_c chosen. In the beginning, if we do not take the correct constellation point, the convergence for the values of the Jone's matrix is incorrect. This is illustrated below, after running the algorithm in a blind manner.

As can be seen by the convergence plots above, the values of a, b, c & d converge, but to values different from the taken values. This means, that although the constellation is restored, it is rotated by an arbitrary phase of $\frac{n\pi}{2}$. In order to avoid this rotation, a known training sequence of known length must be transmitted prior to the data, to converge the Jone's matrix to the right value.

The next chapter goes on to demonstrate the experimental validity of the KF algorithm with the different algorithms to compensate the other impairments as well. It concludes the discussion on KF and EKF for PN tracking and presents future potential areas of extending this work.

Chapter 4

Experimental Validation: KF for PN

This chapter covers the experimental validation of the KF algorithm discussed in Chapter 2. The data to be tested is collected in raw format, in the form of digital complex samples. In addition to polarization tracking and phase noise compensation, other offline DSP algorithms are implemented, which are also clearly mentioned. In addition, different algorithms for phase noise compensation are compared. Conclusions based on the experimental validation are also presented. This chapter concludes the first part of the report, for coherent communication. It ends with the conclusions and future prospects of the same.

4.1 Experimental setup

The schematic of the experimental set up is shown in Figure (4.1). A set of 40 narrow line width lasers spaced $100GHz$ apart are combined by a PM arrayed waveguide grating. Output of another similar grating is combined with the first set of 40 lasers using a PM combiner to produce an optical signal covering the entire C band with 80 optical channels and $50GHz$ separation between neighbouring channels. This optical signal is fed to an optical multi-format transmitter (OMFT) consisting of a pair of IQ-modulators with polarization multiplexing capability. The OMFT is driven by 4 parallel electrical data

channels generated by a $34Gsa/s$ AWG at the rate of $25GBaud$. The modulated PDM-QPSK signal (a PRBS of length of $2^{31}-1$ bits) after passing through a decorrelator, is transmitted over 23 spans, each of length $80km$, of standard G652.D Sterlite OH-LITE fibers with an initial launch power of $0dBm$. The loss of each span($17dB$) is compensated with a variable gain EDFA. No dispersion compensation is used in the link. The received signal is amplified and applied to a phase and polarization diverse coherent receiver.

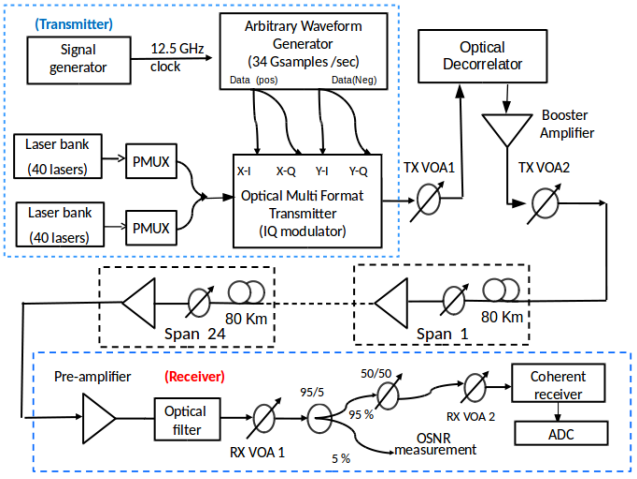

FIGURE 4.1: Schematic of the Experimental Setup

This is followed by a $63GSa/s$ Keysight ADC which captures the in-phase and quadrature-phase data of each polarization in the digital domain.

4.2 Offline processing

The digital data at the ADC output is processed offline to mitigate the effects of channel and system impairments. The detailed description of different algorithms for the compensation of different impairments and the general sequence of their application is well studied in [10]. Polarization de-multiplexing is implemented using a single tap butterfly filter, where each tap is updated using constant modulus algorithm [11]. We use Gram-Schmidt orthogonalization process to compensate for IQ imbalance [12], frequency domain equaliser for CD and fourth power periodogram technique for FO. This is then followed by the compensation algorithm for PN. Here, KF is implemented, using the DD-LMS as a reference. This is given in the diagram below.

The number of symbols that could be processed off-line is limited by the memory of ADC used. Samples corresponding to 7000 symbols are saved multiple times and processed

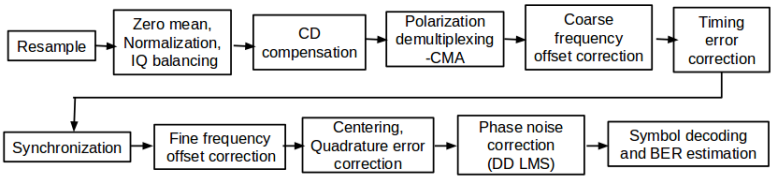

FIGURE 4.2: Sequence of DSP algorithms in offline DSP processing

offline using the modified sequence of DSP for each of the span lengths. Fig. shows the BER measured as a function of number of spans, indicating error-free operation for fiber lengths upto $1840km$.

4.3 PN Compensation

This section provides the experimental results of using KF for PN compensation.

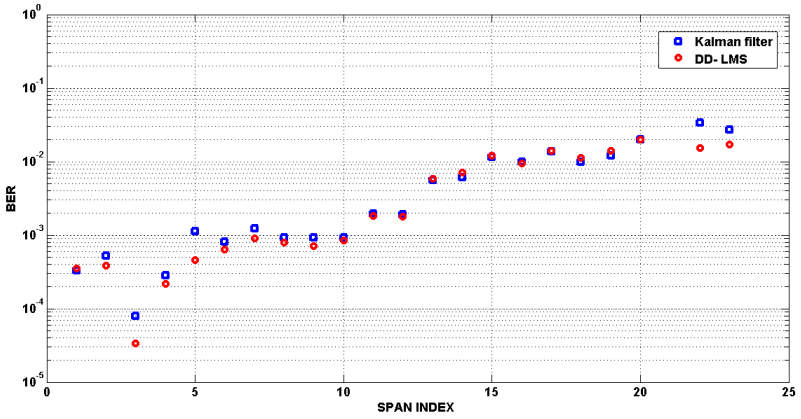

FIGURE 4.3: Variation of BER with span number corresponding to channel frequency of $192.35THz$

The KF was implemented for QPSK modulated experimental data. The Following section presents the BER analysis for a 24 span $25GHz$ data.

- The KF algorithm is carried out as **a blind algorithm**, with the pseudo-training sequence to converge the values of Kalman gain and state covariance
- However, since the algorithm is run in a blind manner, it runs into a problem, when tested with the data
  - Beyond the 14^{th} span, the entire constellation is rotated by $\pi/2$
  - However, this was corrected by removing the IQ imbalance compensation

  - Since the DDLMS and KF, when using a training sequence, are able to compensate for this offset, the DDLMS works in the presence of the IQ imbalance

- The compensation algorithm prior to phase noise correction is optimised for each span, and the same is used before implementing both KF and DDLMS

  - This includes choosing the coefficients for polarization compensation, timing and synchronization

- For KF implementation each parameter Q and R can be individually optimized for each span, but it was kept constant, for a uniform implementation of the algorithm

  - R was fixed to 0.00397
  - Q was fixed to $1.25e-05$

The following table gives a brief comparison of the 2 algorithms.

	DDLMS	**KF**
Training Sequence	10 symbols	No sequence required
Convergence	Filter tap	Kalman gain
OSNR value	Not needed as input	Required to be input for measurement noise
Laser linewidth	Not known	Required to be input for measurement noise
Noise model	Not required	Q and R values decided on the model

TABLE 4.1: Table comparing BER values of the two phase noise algorithms

Based on the analysis of the Kalman Filter for phase noise tracking and compensation, the following conclusions can be inferred:

- The Kalman filter gives the same performance as DD LMS, with experimental as well as simulated data
- The performance of both algorithms is the same, in terms of time taken for execution
- Kalman filtering has the advantage of being executed as a blind algorithm, making use of a pseudo-training sequence as explained
- The KF can be optimized for each data set, depending on the noise properties, however it is a very robust implementation and does not affect the overall order of the BER

4.4 Conclusions and Future Work

This presents the different conclusions and the potential improvement in the algorithms discussed in chapters 2 and 3.

- Both KF and EKF have an excellent agreement with the noise model for compensation, hence they are efficient algorithms for compensation of impairments
- The limitations of both have been clearly highlighted and with respect to the noise models
- Further improvement in the PN tracking algorithm can be obtained by analyzing, in detail, the behavior of the cycle slips and hence modifying the KF algorithm to compensate the errors to unwrap this phase
- The EKF algorithm can be modified to be implemented without the need for a training sequence, to be used in the DSP chain for experimental data
- KF can be additionally used for other impairment compensations like timing recovery, FO detection and compensation, and CD management
- Application of KF can be further extended to integrate with advanced multicarrier modulation like OFDM or Nyquist WDM, to be used in combined demodulation and impairment compensation
- KF is especially useful as it specifically considers the generation and impairment model of the system; it considers the sources of the noise in the system and effectively tracks the state, which makes it a powerful contender for DSP in coherent optical communication
- Effect of other compensation on the phase noise is also a valid distortion and has been excessively analyzed; the KF can be modified to consider such Equalization Enhanced Phase Noise (EEPN) distortions [13] [14] [15]
- Additional analysis of PN algorithms can be done in detail to determine the applicability of each algorithm for different conditions; a systematic comparison of different PN tracking algorithms can be presented

Chapter 5

Underwater Communication Using Optical Paradigm: Introduction

The following chapter introduces the project work done in the field of underwater optical communication. Here effect of digital modulation is investigated in the presence of optical nonlinearities, that cannot be completely characterized as a linear system. The effect of such nonlinear interactions with the optical signal isn't easily quantifiable, as will be shown in the next few sections. The motivation for this analysis as well as the complete system description is provided here. The role of optics in the entire system level implementation is also clearly mentioned. The detailed system level description of each block is presented in the subsequent chapters. The work presents an analysis of signal distortion due to optical nonlinearities, specifically analyzing the *Second Harmonic Generation* (SHG), and a specific digital precompensation scheme for overcoming this distortion.

5.1 Project Overview

Conventional submarine communication has an imperative need for the vessel to resurface to transmit the signal to the base station. However, an effort is being made to

eliminate this need and transmit the signal though the water and then through the atmosphere to the base station.

- A huge part of the analysis involves estimation of the channel characteristics and distortions to the signal
- These same distortions are being analyzed and modeled as a transfer function, which will aid precompensation and postcompensation techniques for the transmitted signal
- The role of optics is in the design of a sustainable optical transmitter-receiver link for this communication

5.2 Optical Transmission: Block Diagram

The "blue-green window" has been identified as the carrier of information for the underwater communication link. This section provides an overview of the system design of the system using lasers operating in these wavelengths.

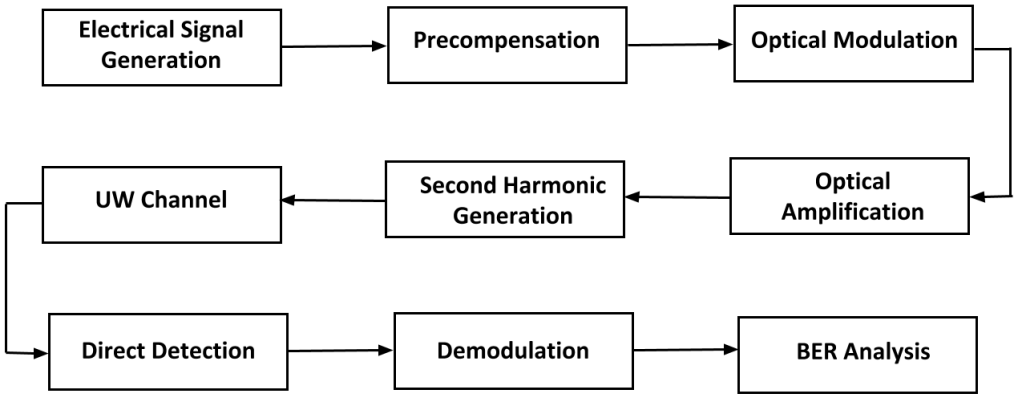

FIGURE 5.1: UW Project System Block Diagram

Electrical Signal Generation: This represents the source of the information to be transmitted.

- The data to be generated is modulated as an electrical RF signal and fed to the modulator
- The data rate is in the range of $100Mbps$
- The specifics of the modulation are also described and elaborated in the following chapters
- For the purpose of the system analysis, two distinct modulation formats are investigated: Pulse Position Modulation(PPM) and Orthogonal Frequency-Division Multiplexing(OFDM)

Precompensator: After signal generation, it has to be specifically precompensated for overcoming the optical nonlinearities

- The signal is still in the electrical domain
- The reason for the precompensation will become evident after explaining the system nonlinearities

Optical Modulation: This step converts the signal to an optical waveform.

- The RF signal is modulated on an optical carrier at $1024nm$
- Optical modulation can be done through direct modulation of the laser or through external modulation using an MZM (Mach Zender Moulator)

The effects of modulation induced nonlinearities are also explained in detail in the next few chapters.

Optical Amplification: The transmitted optical signal is amplified using a standard optical amplifier structure: EDFA(Erbium Doped Fiber Amplifier)

SHG: This block adds the main component of the nonlinearities present in the transmitter.

- Channel analysis done for the underwater medium have shown that the transmitted waveform should be at a wavelength of close to $532nm$
- The transmitter chain generates the data, modulated on an optical carrier, at $1024nm$
- In order to convert to the desired wavelength of $523nm$, the amplified optical waveform is passed through an SHG setup

The detailed effect of he SHG process and the nonlinearities associated with it, after coupling the block with the external modulator has been described in detail in the subsequent chapters. It is to be noted that although the analysis of the SHG is presented, there is no description of the physical system description of the setup. This setup is underway and is soon to be incorporated in the chain as a physical block.

Underwater Channel: Although the main crux of underwater communication is the channel impairments presented, this analysis has been oversimplified. This report specifically shows the effect of the transmitter, SHG and receiver induced nonlinear effects for the optical waveform. However, the channel model has been presented as a simplified AWGN channel. The exact channel response is being separately analyzed by means of physical experimentation in the ocean.

Direct Detection: The received signal is detected by means of optical DD(Direct Detection).

- The received electric field is proportional to the intensity of the optical signal
- This square law detection further imposes constraints on the modulated optical waveform

The effects of the receiver and the constraints presented are also explained in detail in the following chapters

Demodulation: This block involves recovery of the data bit stream from the received electrical signal. The demodulation for the PPM and OFDM is separately carried out

and analyzed further. In addition, after introducing the channel model, the demodulation block will also include compensation algorithms for channel impairments.

5.3 Challenges for Optical Communication

The following are some challenges with respect to the overall optical transmission system.

- SHG is a second order effect and distorts modulation and phase information
- The choice of the precompensation scheme used to overcome all system nonlinearities
- The use of spectrally efficient modulation schemes like OFDM make the system more vulnerable to AWGN
- As explained in the first part of this thesis, laser phase noise is an especially important effect and plays a more major role for lower baud rate systems due to the presence of flicker noise

5.4 Extent of Analysis Done

As an overview of the work done analyzing the system performance of the 2 distinct modulation schemes: PPM and OFDM, the following tasks are done

- The entire chain explained above is simulated to check the performance of the modulation by varying the parameters of the different blocks present
- Preliminary experimental testing is done, without the underwater channel, to shown the working of the modulation and demodulation setup designed
- Validation and analysis of the performance is done by means of analysing the system BER, for different SNR values

Chapter 6

System Description and Simulation: Flip OFDM and L-PPM

This chapter presents a detailed overview of the different system blocks described above. The entire chain is simulated and analyzed by varying different system parameters. This chapter introduces the Flip-OFDM modulation in the underwater communication communication link. The different optical as well as electrical components are also further elaborated. The aim of this chapter is to simulate the entire OFDM system in the presence of the different system nonlinearities. This is followed by the modulation system description for L-PPM. The performance of this system is also evaluated for the same channel, with the SHG nonlinearities. The comparison with the Flip-OFDM system is left for the following chapter.

6.1 System Block Diagram: Flip-OFDM

The following section presents the system block diagram, tracing from the data generation to the final demodulation, as illustrated in the block diagram below.

- The data is generated as a QPSK constellation and then fed to an OFDM block for modulating individual subcarriers

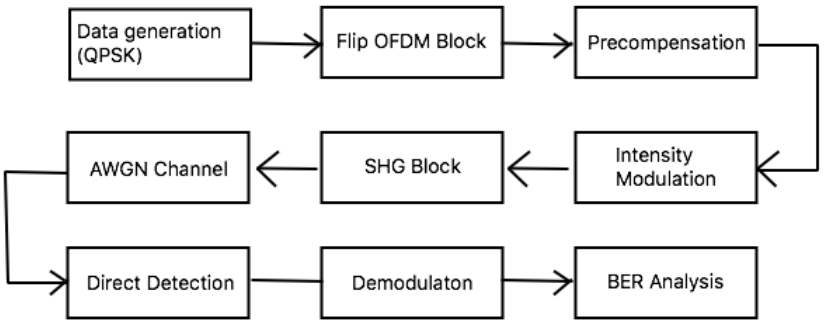

FIGURE 6.1: Flip-OFDM Block Diagram

- The generated OFDM time-domain signal is then input to a Mach-Zender Modulator
- The signal is modulated at 1064nm carrier
- The modulated signal is fed to a SHG block to convert it into a 532nm carrier; however, before passing through the SHG block, it is precompensated for the nonlinear transformation
- The channel is modelled as an AWGN channel with varying SNR levels
- The signal is then directly detected and then demodulated using the same OFDM architecture
- The BER analysis is done to check the resilience of the modulation and the precompensator to the channel

6.2 System Description

The following subsection presents the individual system description of the different blocks of the optical communication module. The following are the different blocks with the mathematical equations defining the input and output of each. In addition, the different parameters taken for the specific implementation are also clearly mentioned.

6.2.1 Flip-OFDM Generation

OFDM system of multicarrier modulation uses the orthogonality property of harmonic multiples of sinusoids to produce a high spectral efficiency communication system. The following figure illustrates the basic OFDM block with M subcarriers.

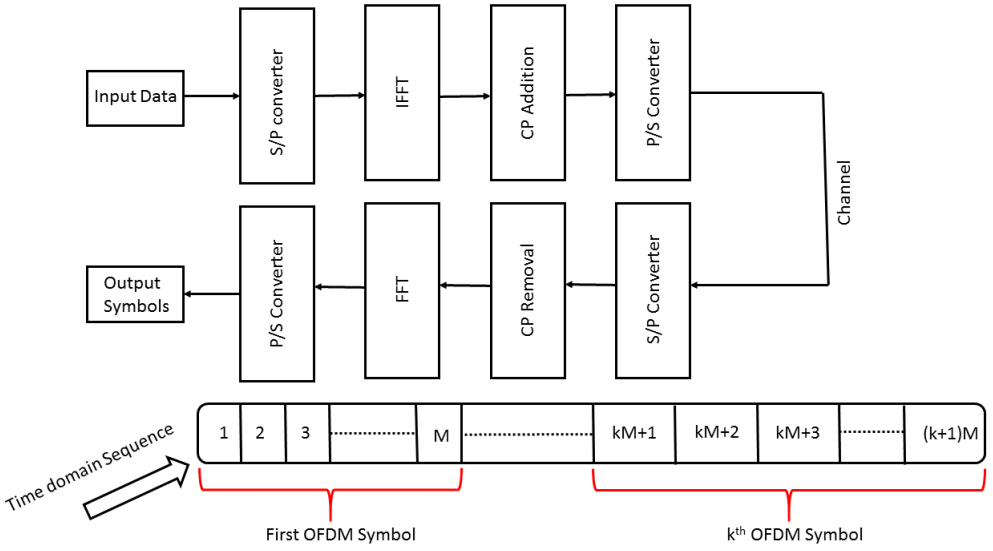

FIGURE 6.2: Flip-OFDM Block Diagram

- The total bandwidth is fixed, depending on the rate at which the data is fed in parallel to the IFFT block: let this data rate be denoted by R_{data}
- If there are M subcarriers, each occupies a subcarrier spacing of $\frac{R_{data}}{M}$
- M symbols are processed in parallel, so the OFDM symbol rate is:

$$R_{ofdm} = \frac{R_{data}}{M} = \frac{1}{M * T_{data}} \tag{6.1}$$

The following shows the spectrum of the OFDM modulation, in comparison to a WDM frequency modulation.

The following are the system requirements:

- For IM, we need to give a real valued time domain signal; in order to generate a real valued signal, Hermitian symmetry is employed
- Half the OFDM subcarriers are modulated independently and the second half is a flipped conjugate version of this half

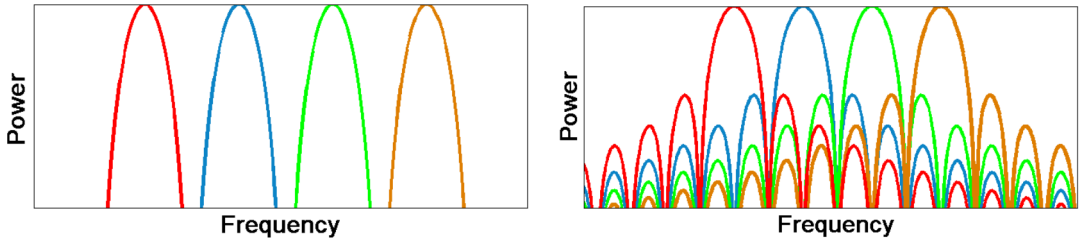

(a) FDM/WDM (b) OFDM

FIGURE 6.3: OFDM Spectral Illustration

- Mathematically writing this equation,
  - The first subcarrier is represented as X_0
  - If the $(k+1)^{th}$ subcarrier is X_k, then the $(M-k)^{th}$ subcarrier is $conj(X_k) = X_k^*$
  - The output of the IFFT is a real-valued sequence
- In order to make the signal more resilient to ISI and channel distortions, we also introduce a guard band on the edges of the signal; this is illustrated a little later

Flip OFDM is used for the SHG test. The reason is to maintain a positive valued signal, the reason for which will become evident in the precompensation block. In order to obtain a real signal, Hermitian symmetry is employed. The OFDM symbol is given by: [16]

$$x[m] = \frac{X_0}{\sqrt{M}} + \frac{1}{\sqrt{M}} \sum_{k=1}^{M/2-1} X_k exp\left(j\frac{2\pi mk}{M}\right) + \frac{X_{M/2}}{\sqrt{M}} exp(j\pi m) + \frac{1}{\sqrt{M}} \sum_{k=M/2+1}^{M-1} X_{M-k}^* exp\left(j\frac{2\pi mk}{M}\right) \tag{6.2}$$

In order to have the DC component equal to zero, we set the symbol values subcarrier 0 and $M/2$ are given zero.

Out of M total subcarriers, there are $M/2-1$ subcarriers which carry useful information. The remaining redundancy is introduced to create the real-valued signal.

Further, to generate a positive signal, the OFDM symbol is split into 2 different signals.

$$x[k] = x^{+}[k] + x^{-}[k] \tag{6.3}$$

$$where, \tag{6.4}$$

$$x^{+}[k] = x[k];\ if\ x[k] > 0 \tag{6.5}$$

$$= 0;\ otherwise \tag{6.6}$$

$$x^{-}[k] = x[k];\ if\ x[k] < 0 \tag{6.7}$$

$$= 0;\ otherwise \tag{6.8}$$

Both $x^{+}[k]$ and $-x^{-}[k]$ are transmitted as separate OFDM symbols with separate cyclic prefixes. The received symbol $y[m]$ is delayed for the OFDM symbol duration and added to the symbol $y[m+1]$. The final received signal is given by

$$y[m] = y[m] - y[m+1] \tag{6.9}$$

The following figure gives a pictorial representation of the modulation for each OFDM symbol.

The following are the parameters taken for the OFDM symbol

- $M = 256$; a total of 256 subcarriers are used for the analysis
- Each subcarrier is modulated using QPSK constellation points A guard band is used: total of 64 subcarriers $(32 * 2)$; the use of a guard band allows for frequency spreading and improves performance due to the SHG
- For Hermitian Symmetry, only half are modulated; the other subcarriers are taken as the conjugate of the first half
- On the basis of the discussion above, the number of useful, independent subcarriers are: $\frac{(256-64-2)}{2} = 95$
- The number of OFDM symbols used: 190 symbols

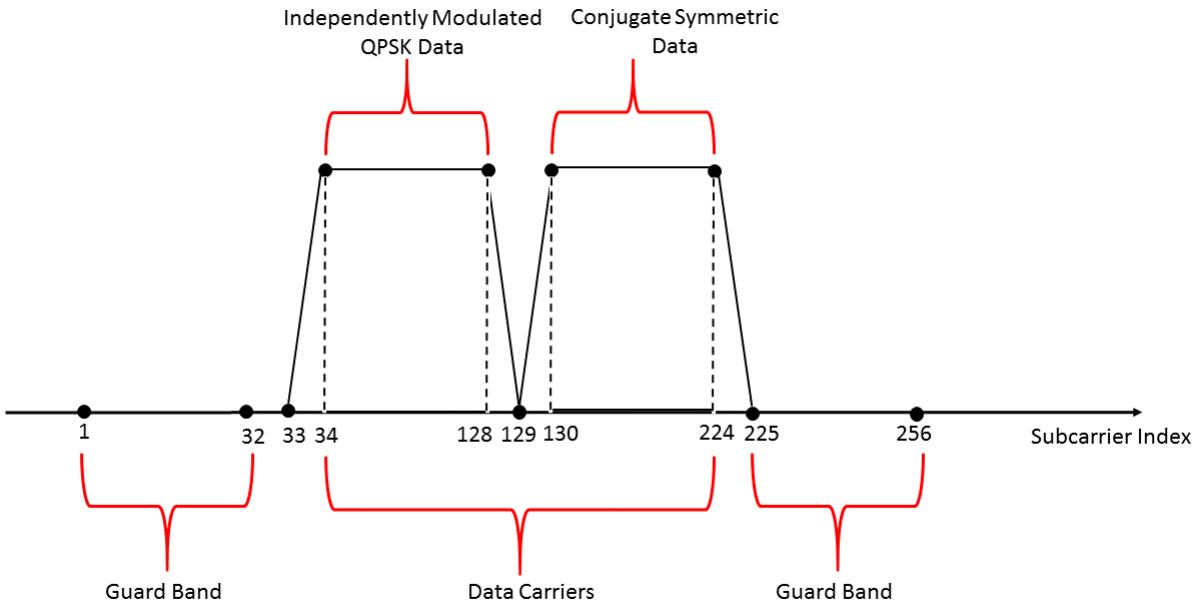

FIGURE 6.4: OFDM Symbol Structure

6.2.2 IM

IM brings the signal from the electrical to the optical domain. We generate and optical carrier at $1064nm$ and feed the Flip-OFDM signal to modulate this carrier. In order to generate an intensity modulated signal, we can use 2 distinct approaches:

1. Direct Modulation
2. External Modulation

In order to generate the output field intensity of a directly modulated laser, we solve the laser rate equations and calculate the output power as a function of the laser input parameters. However, the spectral usage of a directly modulated laser is less efficient than an externally modulated laser. The following two representative plots show the spectrum of an OFDM signal for a directly modulated case vs an externally modulated laser.

- As can be seen from the above representative plot, an external modulation makes results in better spectral utilization

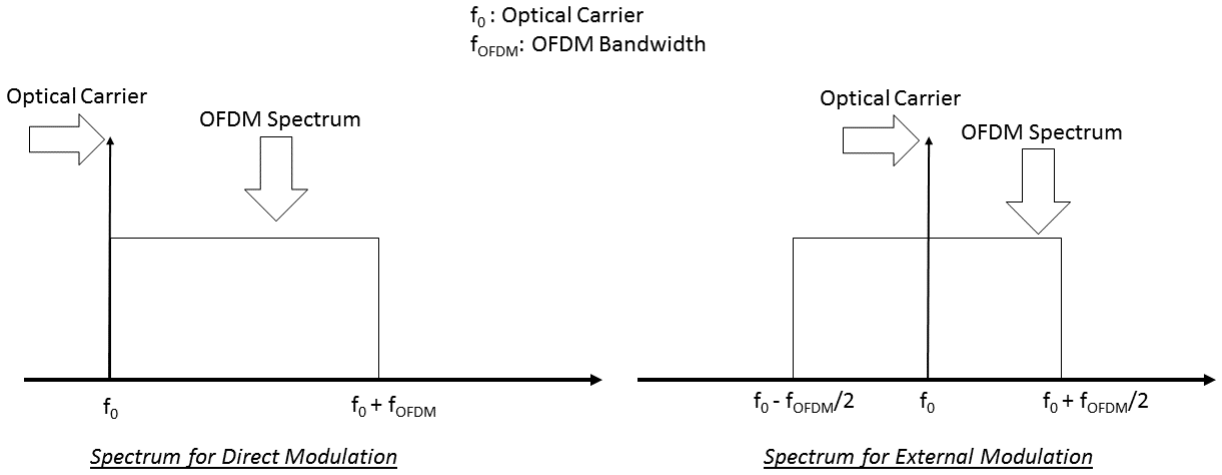

FIGURE 6.5: Spectral Comparison: Direct Vs External Modulation

- For direct modulation, the gain is limited by the laser parameters and bias values
- An external modulation can provide a larger modulation gain when biased appropriately(Elaborated in following parts)
- In addition, the independence of the optical and electrical inputs in the external modulator grant more control over the modulation index and output power separately
- Greater controllability in the carrier and modulation index, along with increased gain makes external modulation a better option for the intensity modulator

The following section goes on to elaborate more on the operation of the external modulator: Mach Zender Modulator (MZM). [1]

The diagram of the MZM is shown below:

The transfer function for the MZM is given as; [17]

$$E_{out} = \frac{E_{in}}{\sqrt{2}}\left[e^{j\Delta\phi(t)} + e^{-j\Delta\phi(t)}\right] = \frac{E_{in}}{\sqrt{2}} cos\left(\frac{\pi V(t)}{V_\pi}\right) \tag{6.10}$$

$$I_{out} = |E_{out}|^2 = 2E_{in}^2 cos^2\left(\frac{\pi V(t)}{V_\pi}\right) \tag{6.11}$$

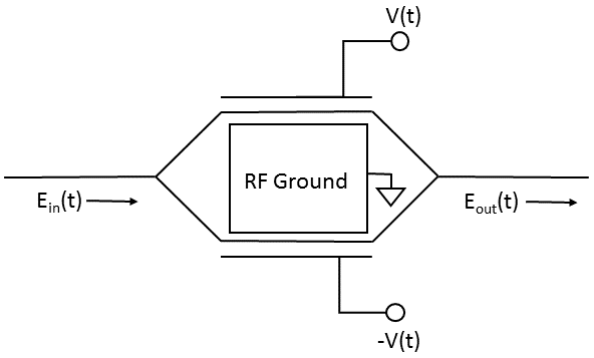

FIGURE 6.6: MZM Diagram

- E_{in} is the input optical field, E_{out} is the output optical field
- The V_{π} is taken as $5V$
- The input optical field intensity is taken as unity
- As mentioned above, the signal $V(t)$ is the suppressed OFDM input to the IM

The following is the plot for the transfer function of the intensity modulator. The output optical field intensity is plotted as a function of the applied RF voltage: $V(t)$. The input field intensity is taken as unity.

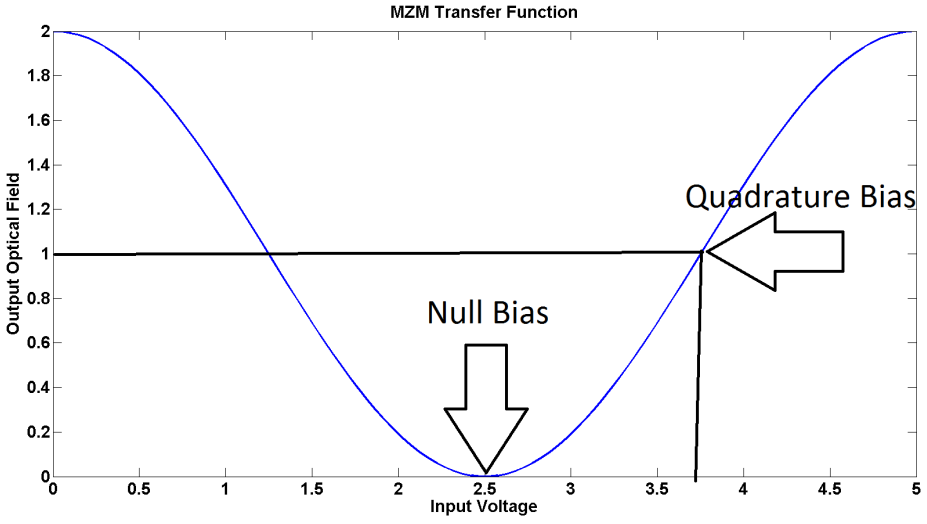

FIGURE 6.7: MZM Transfer Function

The analysis of the signal is presented for the Quadrature Bias and the Null Bias Separately.

6.2.2.1 Quadrature bias: Linear region

When the bias is applied at $7V_\pi/4$, the output is of the form [18]

$$E_{out} = \frac{E_{in}}{\sqrt{2}} cos\left(\frac{7\pi}{4} + \frac{\pi V(t)}{V_\pi}\right) \tag{6.12}$$

$$= \frac{E_{in}}{2}\left[cos\left(\frac{\pi V(t)}{V_\pi}\right) + sin\left(\frac{\pi V(t)}{V_\pi}\right)\right] \tag{6.13}$$

$$for\ V(t) << \frac{V_\pi}{\pi} \tag{6.14}$$

$$E_{out} = \frac{E_{in}}{2}\left[1 + \frac{\pi}{V_\pi} V(t)\right] \tag{6.15}$$

This represents amplitude modulation with unsuppressed carrier

6.2.2.2 Null bias: Nonlinear region

When the bias is applied at $3V_\pi/2$, the output is of the form

$$E_{out} = \frac{E_{in}}{\sqrt{2}} cos\left(\frac{3\pi}{2} + \frac{\pi V(t)}{V_\pi}\right) \tag{6.16}$$

$$= \frac{E_{in}}{\sqrt{2}} sin\left(\frac{\pi V(t)}{V_\pi}\right) \tag{6.17}$$

$$for\ V(t) << \frac{V_\pi}{\pi} \tag{6.18}$$

$$E_{out} = \frac{E_{in}}{\sqrt{2}} \frac{\pi}{V_\pi} V(t) \tag{6.19}$$

This represents the carrier suppressed modulation scheme. However, this cannot be used as the detector requires a carrier component to beat with for DD.

6.2.2.3 Other region

Although the analytical form for biasing the input in a region in between null bias an quadrature bias, is hard to evaluate, the performance of the OFDM in this region is analyzed through the BER Vs SNR plot.

6.2.3 Second Harmonic Generation: SHG

This section gives a theoretical overview of the SHG nonlinearity and the effect on the OFDM signal. It goes on to motivate the use of the precompensator block for the system.

6.2.3.1 SHG: Mathematical model

The main differential equation that has to be solved is the nonlinear Schrodinger's equation for nonlinear fields. [17]

$$\nabla^2\vec{E} - \mu_0\epsilon\frac{\partial^2\vec{E}}{\partial t^2} = \mu_0\frac{\partial^2\vec{P}_{NL}}{\partial t^2} \tag{6.20}$$

The electric fields at ω and 2ω are given as: $E_1 exp(j(\omega t - k_1 z))$ and $E_2 exp(j(2\omega t - k_2 z))$ The value of E_1 and E_2 are given by eq(1). Both these fields have to satisfy the equation above. On putting in the values, two coupled differential equations are arrived at.

$$\frac{dE_1}{dz} = -\frac{j\omega\mu_0 c\alpha}{n^\omega}E_1^*(z)E_2(z)e^{-j\Delta kz} \tag{6.21}$$

$$\frac{dE_2}{dz} = -\frac{j\omega\mu_0 c\alpha}{n^{2\omega}}E_1^2(z)e^{j\Delta kz} \tag{6.22}$$

6.2.3.2 Simplifying assumptions

As an initial analysis, the following assumptions are made.

- Undepleted pump approximation is used, implying, $\frac{dE_1}{dz} = 0$
- As a result of the above simplification, the resulting SHG wave is now $E_2 \sim E_1^2$
- The time dependence of eq(1) is not considered for the simplified case, which will change on using an OFDM signal pulse
- Phase matching condition is ensured; this implies $\Delta k = 0$

6.2.3.3 SHG for a CT sinusoid

The input fed is a sinusoid at $200kHz$. The input and output spectrum of the sinusoid is given below.

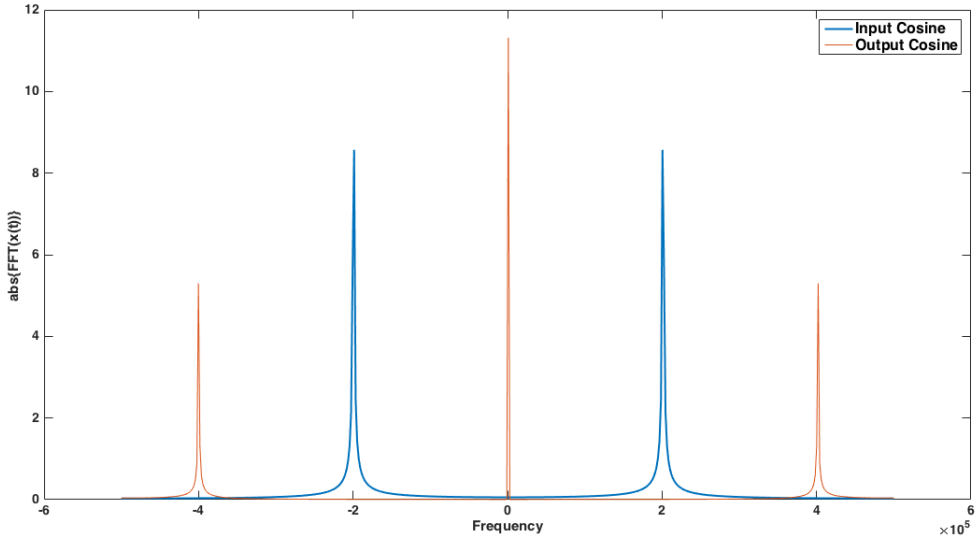

FIGURE 6.8: SHG for CT sinusoid

6.2.3.4 SHG and Flip-OFDM

The Hermitian Symmetric OFDM signal is generated as:

$$x[m] = \frac{1}{\sqrt{M}} \sum_{k=1}^{M/2-1} X_k exp\left(j\frac{2\pi mk}{M}\right) + \frac{1}{\sqrt{M}} \sum_{k=M/2+1}^{M-1} X^*_{M-k} exp\left(j\frac{2\pi mk}{M}\right) \tag{6.23}$$

The output of the system is a signal, proportional to $x[m]^2$

The analytical expression for the subcarrier mixing is given by:

$$E_{SHG}[n] = \left\{ \frac{1}{\sqrt{M}} \sum_{k=0}^{M-1} X_k exp\left(j\frac{2\pi nk}{M}\right) \right\}^2 \tag{6.24}$$

$$= \frac{1}{\sqrt{M}} \left\{ \sum_{k=0}^{M-1} \sum_{l=0}^{M-1} X_l X_k exp\left(j\frac{2\pi n(k+l)}{M}\right) \right\} \tag{6.25}$$

$$= \frac{1}{\sqrt{M}} \left\{ \sum_{k=0}^{M-1} X_k^2 exp\left(j\frac{2\pi n * 2k}{M}\right) + \sum_{l=0}^{M-1} \sum_{m=0, m\neq l}^{M-1} X_l X_m exp\left(j\frac{2\pi n(l+m)}{M}\right) \right\} \tag{6.26}$$

In the above equation, the second expression represents the cross terms; in order to recover information, we need to do prefiltering to avoid intermixing of the subcarriers on convolution, to recover each individual X_k

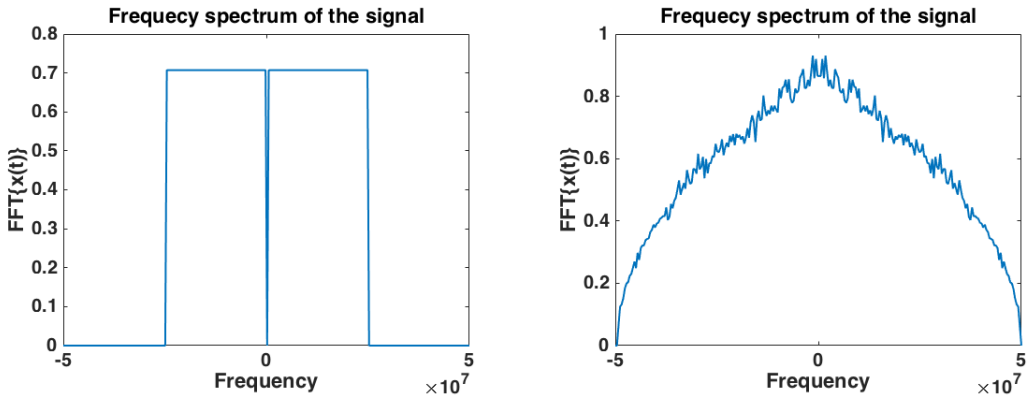

FIGURE 6.9: Effect of SHG on OFDM Spectrum

- The multiplication of the signal in the time domain, implies that there is convolution in the frequency domain
- As a result of this convolution, the bandwidth of the signal will be double of the input signal
- The information in each subcarrier will no longer be preserved as the symbol X_k but will be a mixing of the different frequencies

The presence of this second order nonlinearity, in addition to the modulator characteristics, means that there is a need for precompensation to maintain the spectral properties of the OFDM signal. This is further discussed ahead.

6.2.4 Precompensation

Since the output of the SHG squares the electrical signal, the input fed in to the IM is the square root OFDM signal. The output of the SHG for a quadrature biased IM is now of the form:

$$E_{SHG} = \frac{E_{in}^2}{4} e^{j2\omega t} \left[1 + m\sqrt{V_{OFDM}(t)}\right]^2 \tag{6.27}$$

$$E_{SHG} = \frac{E_{in}^2}{4} e^{j2\omega t} \left[1 + m^2 V_{OFDM}(t) + 2m\sqrt{V_{OFDM}}(t)\right] \tag{6.28}$$

The use of flip OFDM is warranted here as we are taking the square root of the output signal.

As opposed to using a normal signal, the square root precompensator reduces the subband interference noise as these components are suppressed during direct detection. The performance of both are compared in the plots given while analyzing the performance.

6.2.5 AWGN channel

The channel introduced is an AWGN channel with zero ISI. The noise power is calculated based on the signal power, as the SNR is varied from 5dB to 30 dB. Some salient features of this AWGN channel to consider while choosing the bias point are as:

- The quadrature bias has a maximum carrier component, so the signal is much more susceptible to the AWGN channel as the modulation index is small
- We cannot completely suppress carrier because it is needed for DD; operating near the null bias region will reduce carrier component, however a linear model for the output signal cannot be used
- However, by reducing the carrier components, we have a larger subband interference as the term $V^2_{OFDM}(t)$ will have a larger contribution and will increase the noise
- The trend observed is an improvement in performance as we move towards the null bias region of the IM

6.2.6 Direct detection

The direct detection of the optical field involves the detection of the optical field intensity. Therefore, the output intensity of the modulator is given as:

$$E_{out} = \frac{E_{in}}{\sqrt{2}}\left[e^{j\Delta\phi(t)} + e^{-j\Delta\phi(t)}\right] = \frac{E_{in}}{\sqrt{2}} cos\left(\frac{\pi V(t)}{V_\pi}\right) \tag{6.29}$$

6.2.6.1 Quadrature bias

The output optical field when biased in this region is given by the following equation, provided the small signal swing is low compared to V_π

$$E_{out} = E_{in}(1 + m.V(t)) \tag{6.30}$$

Here, m is the modulation index and $V(t)$ is the input electrical signal(in this case, the OFDM signal).
Let the input OFDM have M subcarriers. The data on each subcarrier is denoted as B_k. The received signal is proportional to the electric field intensity and is of the form: [18]

$$I_{rx} = A\left[\sum_{k=1}^{N} cos\left(\frac{\beta_1 + \beta_2 - 2\beta_3}{2} z\right) B_k\right] \; + \; B\left[\sum_{k=1}^{N} B_k\right]^2 \; + \; C \tag{6.31}$$

- The constants A, B and C are dependent on the attenuation, the responsivity of the detector and the input field power
- β_1, β_2 and β_3 are the propagation constants $\beta(\omega_0 + k\Omega), \beta(\omega_0 - k\Omega)$ and $\beta(\omega_0)$ respectively; these depend on the propagation of the wave though a distance z of the fiber
- Because of the propagation, each subcarrier is further multiplied by a Frequency Fading coefficient which can be precompensated
- The second term of $eq(6.31)$ represents the subcarrier-to-subcarrier interference
- The third term is the DC term
- One of the main limitation of operating in the linear region is the large extinction ratio between the carrier and the data spectrum; the energy in the carrier is wasteful as it does not contain any useful data bits

6.2.6.2 Null bias

For direct detection, we need a carrier component to beat with the tones at subcarrier frequencies to generate the signal. Hence we cannot have perfect null biasing. However,

we bias it close to the null to ensure some carrier component. However, the trade-off is operating in the nonlinear region. The analytical model isn't presented here, but the performance plots show the effect of biasing close to the null.
If we use only Hermitian symmetric OFDM, the signal voltage can take both positive and negative values; if we bias at a point very close to the null, the swing of the input voltage will cause two distinct OFDM signal values to take the same intensity value. However, we can avoid this problem by considering the Flip OFDM signal that will take only positive values and not cause this problem.

6.3 Simulation of Flip-OFDM System

The following section describes the simulation of all these blocks put together. A spectral analysis is presented, which further elaborates the effect of the nonlinearities. Following this the system is evaluated on the basis of BER for different receiver SNR values.

6.3.1 System assumptions

The following are the simplifying assumptions for the implementation of the different blocks described above. The assumptions made are for the system simulations conducted in Matlab.

- The normalizing constants are taken as unity for the SHG case
- The undepleted pump approximation and the phase matching for SHG presents the process as a simple square law process
- The time domain parts of the pulse is not considered
- The propagation effects of the wave through the gain medium are also not considered
- The responsivity of the detector is also taken as unity
- Both the MZM and the detector are assumed ideal with infinite extinction ratio

6.3.2 Performance evaluation

The implementation of the specific model as described above is carried out with an AWGN channel. The performance is gauged in terms of the BER measured for the different values of the SNR.

The reference plot is plotted as an all electrical signal. No IM, SHG, Precompensation or DD is done. The OFDM signal is generated, passed though an AWGN channel and then demodulated.

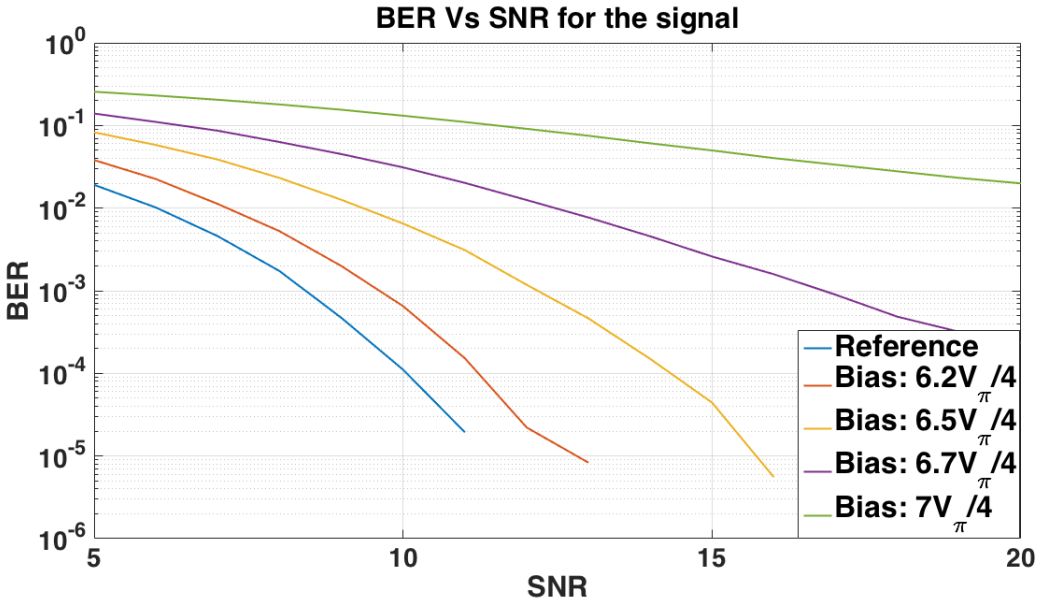

FIGURE 6.10: Performance with varying system bias

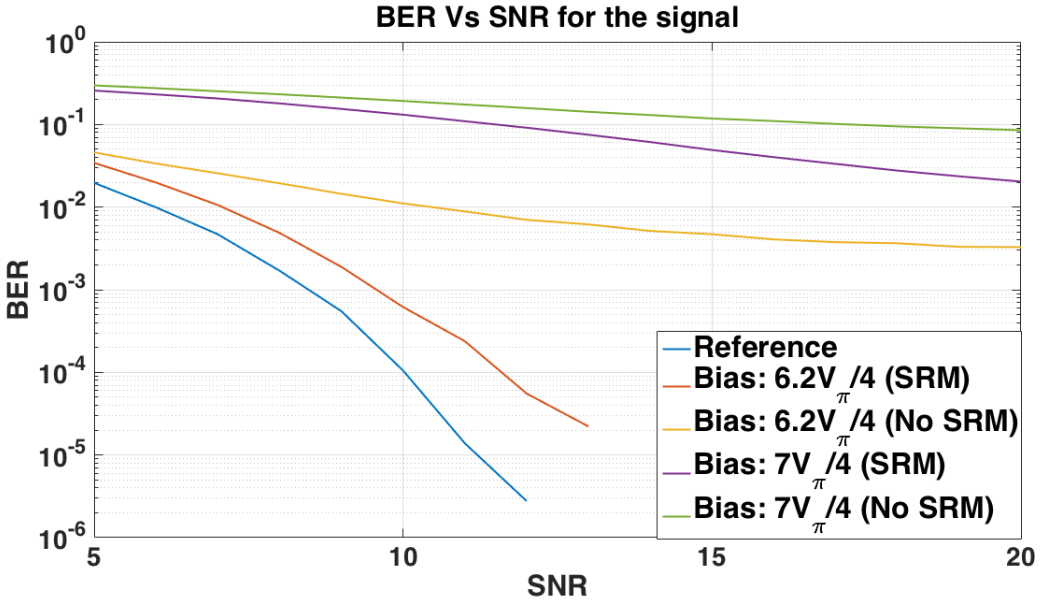

FIGURE 6.11: Performance improvement with the Square Root Module(SRM)

- The first plot shows the performance of the system at different bias values using the precompensation block
- The second plot shows the advantage of using the precompensator
- The improvement in performance as we near the null bias region is evident is consistent with the AWGN definition given above
  - With quadrature bias, the majority of the signal power is in the carrier so the noise floor for the same SNR value is closer to the OFDM signal level
  - As we near null bias, majority of the signal power is in the useful signal and for the same SNR, the noise floor is much lower

6.4 L-PPM: System Description

The following section outlines the Pulse Position Modulation scheme for transmission. A specific L-PPM format is described. In order to implement this, a direct modulated laser is used along with direct detection. The entire block diagram and the parameters of the modulation are highlighted along with the limitations. The next section focuses on the performance of this system. The performance of the PPM system is compared to the OFDM case for different modulation bias and input swing values.

6.4.1 L-PPM system design

Pulse position modulation modulation is a simplified form of modulation where the power level of the signal can take 2 amplitudes only. The modulation maps a sequence of bits to a PPM chip signal. The transmitted signal is a sequence of pulses. Each pulse has the same amplitude and width, but depending on the bit sequence, the delay between the pulses is changed.

6.4.1.1 L-PPM encoder

In L-PPM, each symbol is represented as a PPM chip, which can take one of two possible values.

- A sequence of L PPM chips corresponds to a PPM symbol
- Each PPM symbol is mapped by $log_2 L$ bits
- If the bit rate is R_b, then the PPM chip rate, i.e, transmitted symbol rate is given by

$$R_{symbol} = \frac{R_b}{log_2 L}$$

- The design of the chip sequence is though an orthogonal basis of an L-dimensional vector space
- The following table illustrates the mapping for 4-PPM sequence, i.e, $L = 4$

Bits	**4-PPM chip Sequence**
00	1 0 0 0
01	0 0 1 0
10	0 1 0 0
11	0 0 0 1

- The same is represented below pictorially

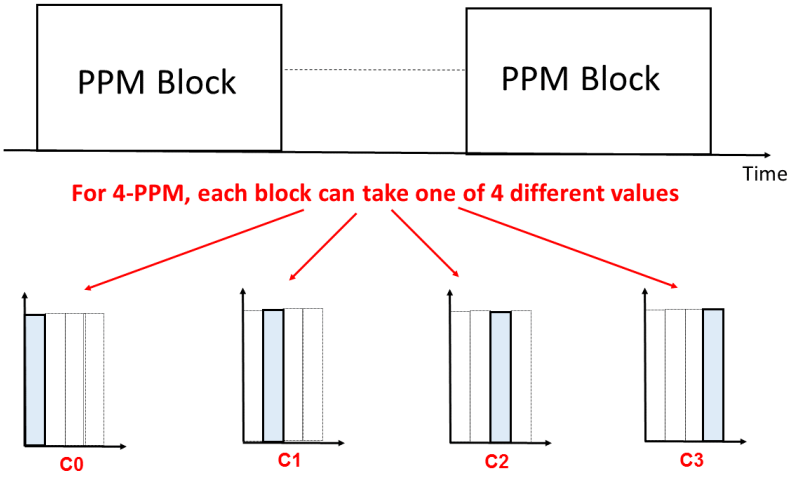

FIGURE 6.12: L-PPM Symbol Structure

6.4.1.2 L-PPM decoder

In order to decode the time domain signal to get the bit stream, we use the orthogonality of the L-dimensional PPM symbol.

- The signal is processed in blocks of size L
- The received noisy signal(of length L) is then split into parallel streams
- Each of these is then correlated with the noiseless chip sequence, i.e the dot product is taken with each of the basis vectors
- The basis which gives has maximum correlation with the input block, is chosen and the bits are decoded as shown in the table above
- A pictorial representation of the same is shown below

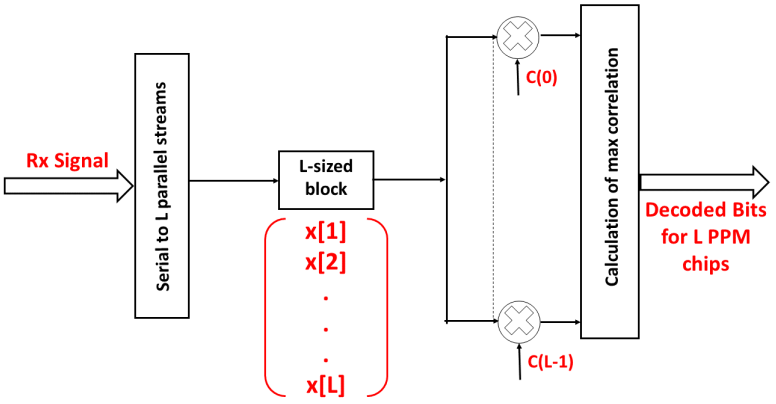

FIGURE 6.13: L-PPM Demodulator

6.4.2 L-PPM system implementation

The following section shows the entire communication link and the different blocks for PPM implementation.

6.4.2.1 Block diagram

The system block diagram is shown below.

The significance of the USRP block will be explained in the following chapter while discussing the experimental validation.

6.4.2.2 L-PPM parameters

The following are the L-PPM Parameters used

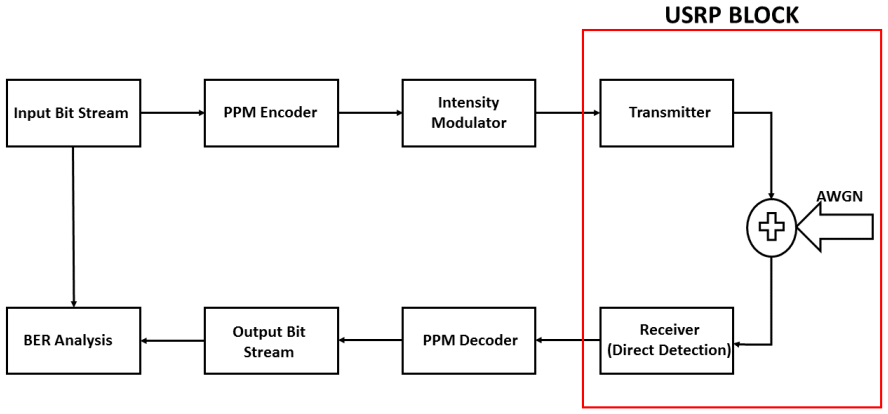

FIGURE 6.14: L-PPM block diagram

- A total of 2048 bits are transmitted
- The value of L is varied as 4, 8 and 16
- The remaining parameters are related to the intensity modulator and the bias values, as are explained below

6.4.2.3 Intensity modulator

The direct modulation of the transmitter laser is given by the following transfer function for the output optical power as a function of the input current.

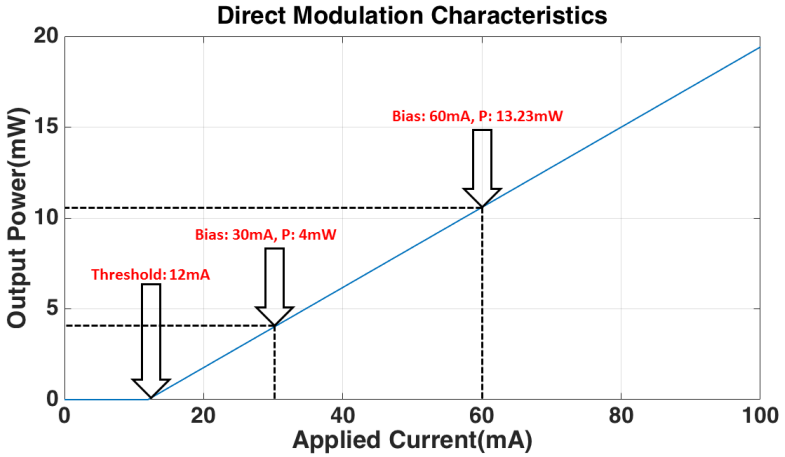

FIGURE 6.15: Direct Modulation Transfer Function

- The threshold value is $12mA$

- The linear transfer function for the current is given as:

$$P_{out} = \frac{15}{68}(I_{elec} - 12)$$

- The values are taken based on certain reference values for direct modulators
- In order to apply the bias and the swing, the value of the PPM signal is normalized with respect to the maximum power and then multiplied by a swing factor to show the effect of the swing and the bias
- This plot also shows the different bias points considered for analysis in the performance section
- Although not shown in the plot, there is an upper limit on the bias current to remain in the linear region of operation, this is taken as $100mA$

6.4.2.4 SHG block

The SHG block is the same as the previous cases for OFDM. The system assumptions for the phase matching, undepleted pump approximation and time dependence still hold true.

$$E_{SHG} = E_{in}^2$$

6.4.2.5 Precompensator

The difference between L-PPM and Flip-OFDM is that in the latter, the amplitude levels are modulated. For L-PPM, just a high or a low level indicates the presence of a signal. Hence, even a squaring operation does not affect the modulated data. With reference to this, it is evident that there is no need of an external precompensator as only the presence or absence of a pulse conveys the information, as opposed to the actual amplitude of the pulse. This is one of the main differences between the L-PPM and the Flip-OFDM modulation. This will further be elaborated in the following chapter.

6.4.2.6 AWGN channel

Here again, the same AWGN channel is used for performance evaluation of the modulation scheme.

- For a given SNR value, the noise floor is given by the $\frac{P_{sig}}{SNR}$
- This noise floor defines the noise variance(noise power): an array of Gaussian distributed values with this variance is then added to the optical signal
- Since the Direct Optical Modulation is used, the optical power is a function of the applied bias and the input swing of the PPM signal
- Since the signal takes only 2 values, the optimal performance is reached by making the swing as large as possible and keeping a lower optical power
- However, the value of the signal power and the swing voltage also determines the nonlinear functionality of the power amplifier, so the values chosen must also consider the power amplifier behavior

6.4.2.7 Direct detection

The direct detection is used, which detects the intensity of the input optical field. For convenience, the responsivity is considered as unity.

6.5 Performance of the L-PPM system

The following section presents the SNR Vs BER analysis for the L-PPM system, as a function of the different system parameters.

The first plot shows the performance of a L-PPM system with varying bias values and input voltage swings.

- As is expected from the behavior of a direct modulated system, the performance is maximum for an infinite extinction ratio with as large a swing as possible

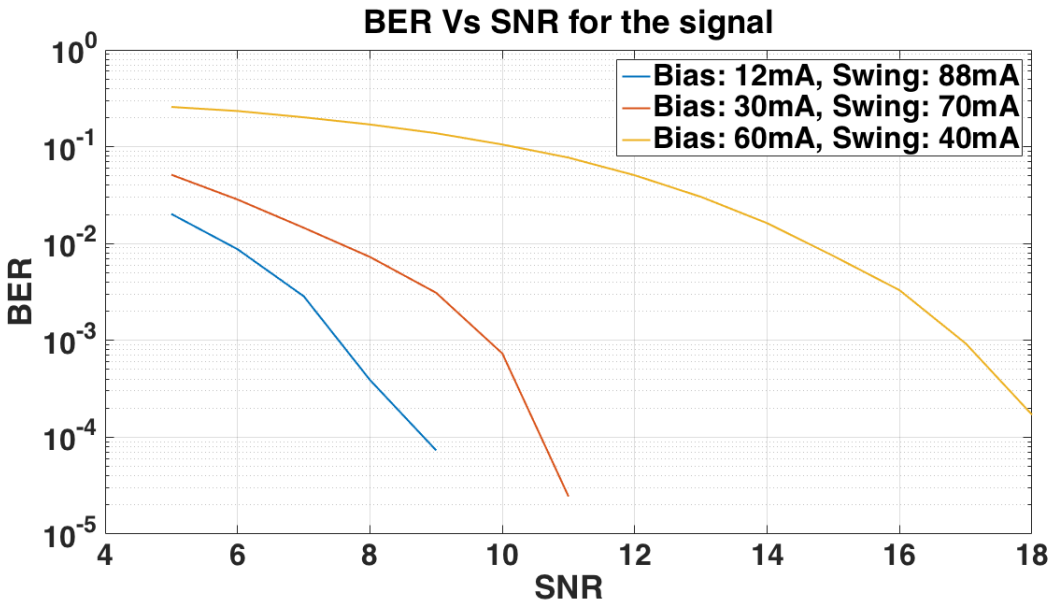

FIGURE 6.16: L-PPM Performance with IM Characteristics

  - The plot corresponding to a bias of $12mA$ and a swing of $88mA$ corresponds to this behavior, in reference to the IM graph
  - However, this means that we transmit zero power when transmitting a zero bit, which is not feasible for real systems

- When we increase the bias, we compromise on the extinction ratio for the system, which makes it more vulnerable to AWGN, this is also illustrated as we increase the bias and keep a larger swing
- The worst performance is observed for a high bias and low swing, as in the case with bias at $60mA$ with a wing of $40mA$
- An optimal approach to direct modulation is to keep a lower bias value with a large input small signal swing

The next plot shows the improvement in the system performance with increasing values of L. The bias current is fixed at $30mA$ and the voltage swing is taken as $70mA$

- As is expected, we see an improvement in performance with increasing L values
- This is attributed to the fact that with an increase in L, the distance between subsequent pulses increases and makes it more resilient to noise; however, long DC values may not be desirable in practical systems

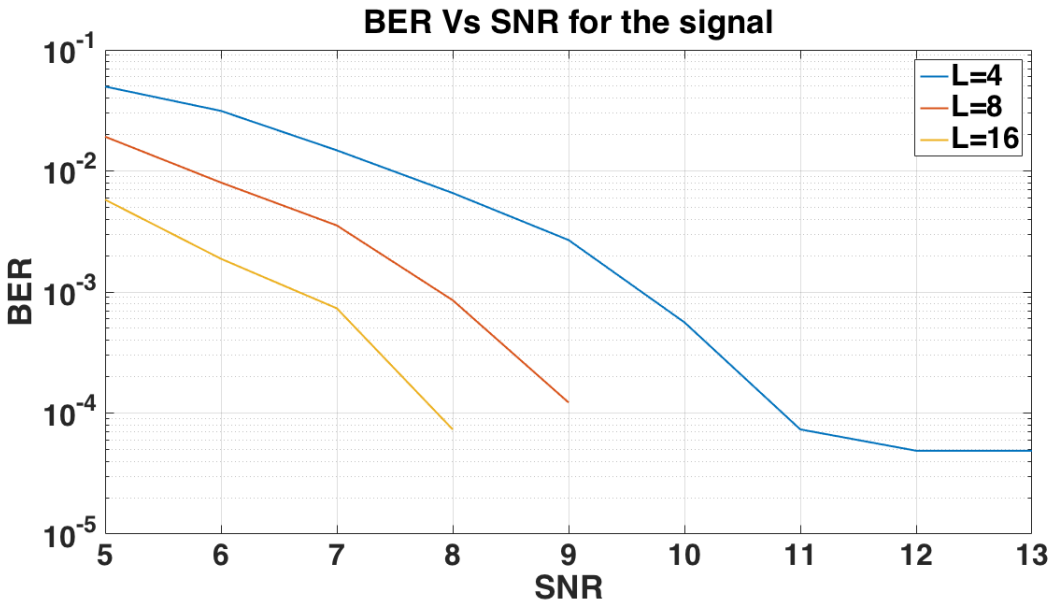

FIGURE 6.17: L-PPM Performance with Varying Values of L

This next chapter presents the comparison of this L-PPM system with the Flip-OFDM system and the different system limitations for each.

Chapter 7

Comparison of L-PPM and Flip-OFDM for Underwater Communication Systems

The previous chapter concluded with the performance characterization of the L-PPM and the Flip-OFDM modulation, individually, for the desired system. Through this chapter, a structured comparison is presented, highlighting the strengths and the trade-offs for using both the modulation formats and the optimal conditions for the use of each. The chapter begins by comparing the performance of the 2 modulations for the desired system. The spectral properties of the 2 systems are also further illustrated. It goes on to highlight the limitations of each modulation, specifically while considering the nonlinearities induced by the SHG. Finally, some concluding remarks are presented from the aspect of implementation of the physical systems for both these modulations.

7.1 Comparison of System Performance

In the previous section, the performance for both the systems was individually analyzed. The performance plots were given by varying the individual system performance. This section now goes on to compare the modulations.

The following plot shows the performance comparison for Flip OFDM and L-PPM.

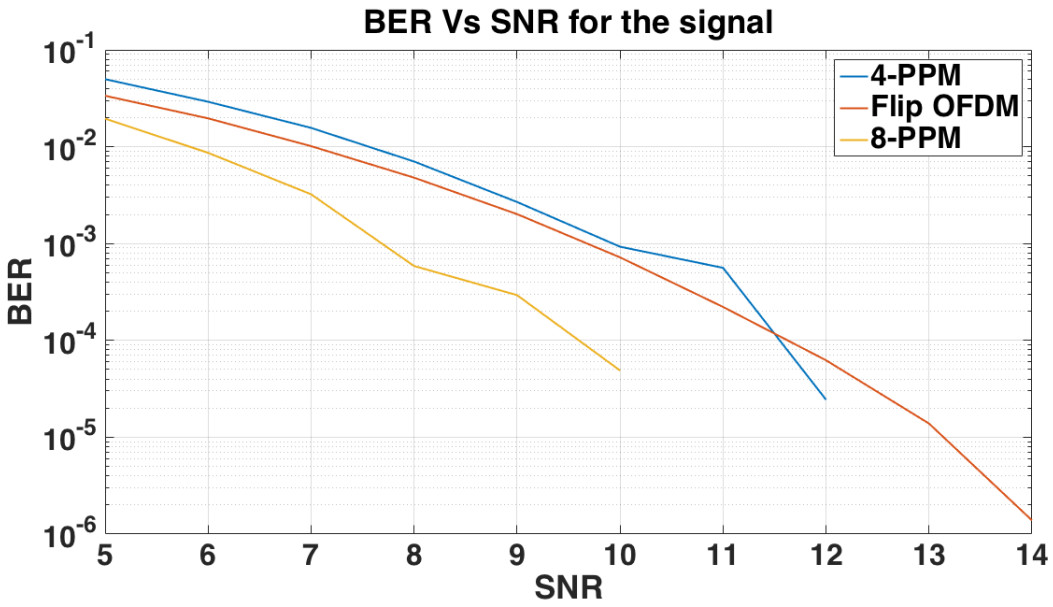

FIGURE 7.1: Comparison of Flip-OFDM and L-PPM

- The performance metric to be measured is the final BER analysis for the same SNR of the generated optical signal
- The OFDM modulation is optimized by biasing the external modulator close to the null region to reduce the effect of sub-band interference
- The comparable performances of 4-PPM and OFDM is an empirical result and can be attributed to the different factors
  - The OFDM subcarriers are modulated with a QPSK signal and are more resilient to the noise as compared to the 1-D(Only 2 intensity levels) PPM signal
- The improvement in performance over 8-PPM is at an additional cost of a reduction in data rate
- Since the effect of the increasing L has other effects for the time domain signal, the analysis discussion is incomplete without the entire system structure
- However, the preliminary analysis done does present with an understanding of the tradeoff of using PPM over OFDM

7.2 Spectral Efficiency Comparison

The following section shows the bandwidth utility of the 2 different modulation formats. Before comparing the performance, the parameters for the modulation are clarified.

7.2.1 System parameters

The symbol rate of both the modulation formats is taken the same. This is so that, theoretically, the 2 occupy the same bandwidth. The bandwidth occupancy is taken as $100MHz$.

- L-PPM Parameters
  - The value of L is taken as 4
  - Bandwidth of $100MHz$ corresponds to a symbol rate of $100MSamp/sec$
  - Following the L-PPM structure of the previous chapter, we have a bit rate of:

$$R_{samp} = 100MSamp/sec \tag{7.1}$$

$$R_{symb} = \frac{R_{samp}}{L} = 25Msymb/sec \tag{7.2}$$

$$R_{bit} = R_{symb} * \log_2 L = 50Mbps \tag{7.3}$$

  - Thus, for a 4-PPM system, a bandwidth of $100MHz$, only corresponds to a bit rate of $50Mbps$
- Flip-OFDM Parameters
  - A total of 256 subcarriers are taken, each being modualted with a QPSK constellation symbol
  - The bit rate for this system is calculated in accordance with the previous chapter as well

$$R_{data} = 100MSamp/sec \tag{7.4}$$

$$R_{bit} = R_{data} * 2 = 200Mbps \tag{7.5}$$

  - However, this is for the ideal case of all independently modulated subcarriers; the previous chapter illustrated that after considering a guard band and Hermitian symmetry, only 95 subcarriers could be independently modulated

$$Useful\ data\ rate = \frac{95}{256} * 200 = 74.21875kbps \tag{7.6}$$

  - The use of Flip-OFDM warrants the transmission of 2 distinct OFDM symbols for maintaining a positive valued signal, further reducing the data rate by half
  - The bandwidth of $100MHz$ gives an effective data rate of $37.109375Mbps$

- However, by eliminating the guard band, a maximum data rate can be increased

$$Useful\ subcarriers = \frac{256-2}{2} = 127\ per\ OFDM\ symbol \tag{7.7}$$

$$Useful\ data\ rate = \frac{127}{256} * 200 = 99.21875kbps \tag{7.8}$$

  Since Flip-OFDM,

$$effective\ data\ rate = 49.609375kbps \tag{7.9}$$

  So a maximum of $49.609375kbps$ can be obtained by eliminating the guard band

- In addition, the individual subcarrier spacing is:

$$\frac{bandwidth}{M} = \frac{100MHz}{256} = 390.625kHz \tag{7.10}$$

7.2.2 Spectral plots

The figure (7.2) shows the spectral plots for the L-PPM as well as the Flip-OFDM, with the parameters defined as above.

- Both the spectra are show with respect to a carrier modulation
- Both the spectra have presence of sidelobes, however, for the L-PPM, most of the information is not contained in the main lobe, marked above
- For the Flip-OFDM, all the information is encoded in the 256 subcarriers, as the signal is defined in the frequency domain

- The OFDM spectrum is more compact and efficient, with respect to information content in the frequency domain

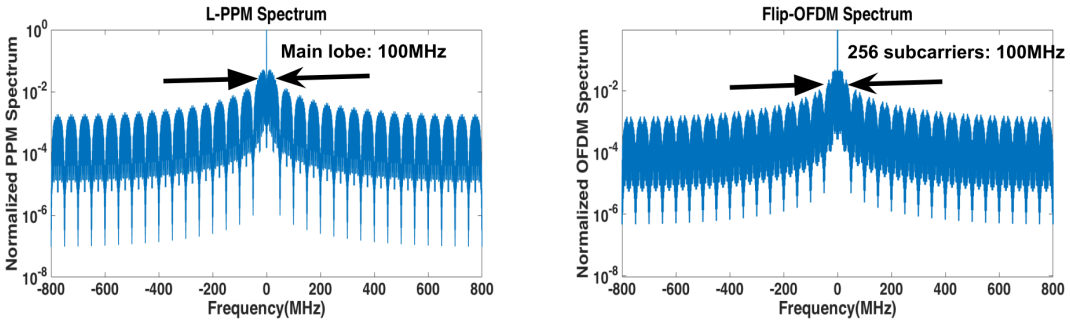

(a) (b)

FIGURE 7.2: Spectral Comparison: L-PPM and Flip-OFDM

7.3 Modulation Limitations

The following section summarizes the limitations of both the modulations, with respect to implementing the system.

7.3.1 L-PPM

Although the L-PPM scheme is a reliable basic noise resistant modulation, there are a few limitations for using this.

- Pulse values only take a high or a low value, so it cannot be used to modulate spectrally efficient formats
- For a fixed symbol rate, we have to transmit L PPM chip sequences, encoding only $log_2(bits)$; this is not an efficient use of the bandwidth for higher values of L(Shown below)
- For larger values of L, the PPM symbol is constant low for a long duration, as can be seen below; this again may not be advisable as it sharply increases the PAPR
- Bandwidth efficiency can be increased by using TDM, but this reflects in increased receiver complexity
- The most important limitation is the lack of spectral control

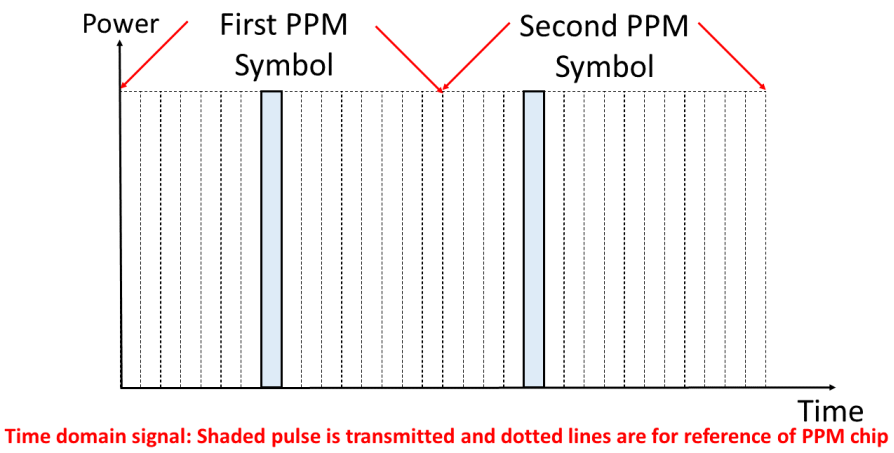

FIGURE 7.3: Illustration of inefficient use of bandwidth for $L = 16$

- For traditional fading channels, the response is not flat over the different frequencies; it has a frequency dependence
- Unlike OFDM [19] the PPM scheme cannot control the spectral behavior of the signal; the value of L should be increased to make it more reliable for a frequency dependent channel
- This is the most important consideration considering the advantages of frequency domain modulation for underwater channels which have a very dynamic frequency response

7.3.2 Flip-OFDM

Although the Flip-OFDM signal presents a spectrally controllable signal, with the modulation being adaptable to the channel in use, there are a few limitations with this modulation format as well.

- Optically, the Flip-OFDM is more difficult to implement; as the amplitude levels are individually modulated, the laser to be used should be a CW laser, as opposed to a pulsed laser
- The time domain signal has more uncertainty as opposed to the L-PPM signal
  - It was shown that the 4-PPM symbol takes only 4 unique values, depending on the bit stream, however the OFDM symbol can take a much larger number of values, depending on the modulation of the subcarriers

  - This uncertainty further adds to the randomness of the time domain signal while modeling noise and nonlinearities

- Although there are 256 subcarriers, as illustrated in the previous chapter, due to Hermitian Symmetry, we can only modulate 95 subcarriers independently; in addition the need to transmit the positive and negative signal separately, further reduces the data rate by half

- An additional precompensator block is required for SHG nonlinearites that are present

  - The Square Root Module for precompensation is necessary to avoid the spectral distortion of the signal due to SHG

  - The L-PPM transmits information by the presence or the absence of the pulse and hence no precompensation is required

7.4 Summary

The following table summarizes the differences, strengths and limitations of using L-PPM as well as Flip-OFDM for underwater communication systems.

Parameter	L-PPM	Flip-OFDM
Modulation	Binary: presence or absence of pulse	Amplitude Modulation
Spectrum	Side lobes beyond spectrum	Spectrally compact: first generated in frequency domain, then converted to time domain
Laser	Pulsed laser can work	CW laser required
Modulation Control	PPM is a fixed modulation	Individual subcarriers can have different modulation
Max Data Rate	Fixed once L is fixed	Can be increased by using spectrally efficient modulation on individual subcarriers
Spectral Control	No spectral control of modulation	Individual subcarriers can be prefiltered depending on channel response
Noise Resiliance	Two amplitude levels so greater resiliance	Amplitude modulated waveform: More susceptible to noise
Transmitter Nonlinearities	Direct Modulation: Linear transfer function	MZM: Linear for quadrature bias, however nonlinear as bias approaches null
SHG Effect	No precompensation	Separate Square Root Module precompensator block required
Demodulation	Correlator based: Complexity increases with larger L	Fixed size FFT matrix for fixed number of subcarriers, independent of individual modulation

Table 7.1: Summary for comparison for L-PPM and Flip-OFDM

Chapter 8

L-PPM and Flip OFDM: Experimental Validation

This chapter presents the experimental work done for verifying the Flip-OFDM and L-PPM modulation and demodulation algorithms discussed for a simplified channel. Although this is preliminary experimental work, the analysis presented will be the basis for more detailed experiments for validation of SHG for the underwater channel. This chapter ends with the concluding remarks and the future work for the underwater communication project.

8.1 Experiment 1: All RF Back-to-back Link Validation

This first experiment is used for the validation of the L-PPM and Flip OFDM modulation and demodulation block for a simple, RF back-to-back case. Although there is no optical modulation, SHG or direct detection for this block, there are quite a few assumptions system design parameters that are important and carried forward for the subsequent optical experiments as well. These are based on the transmitter constraints for the experiment.

8.1.1 Description and block diagram

The following shows the top level block diagram for this experimental transmission.

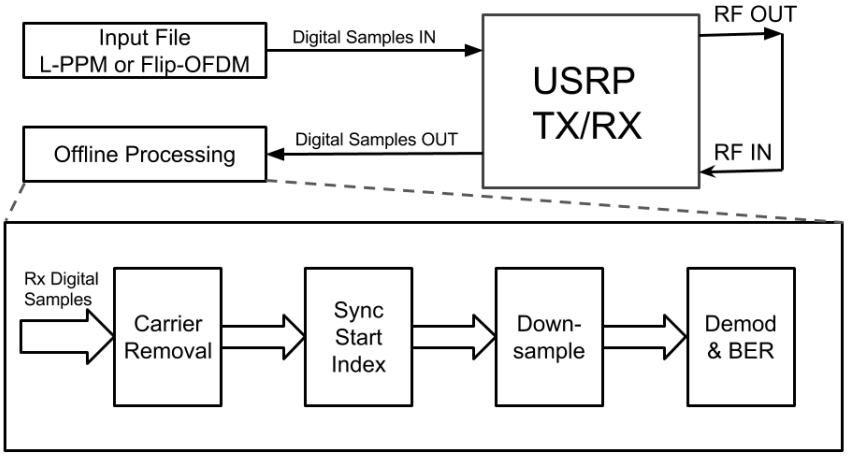

FIGURE 8.1: Overall Block Diagram

The system is described as follows:

- The RF transmitter and receiver used is the USRP N210 baseband board
- The USRP is interfaced with the computer using the GNURadio software module
- All offline processing is written through custom defined scripts, written in Matlab
- The data to be transmitted is stored in a binary file, read by the GNURadio and then transmitted by the USRP
- The files for L-PPM as well as Flip-OFDM have fixed data lengths, and are further described in subsequent sections
- The data is continuously transmitted in a loop and the different capture and synchronization of the start of the sequence is accounted for thought the offline processing, all explained further

8.1.2 System limitations

One of the major system limitations faced while using the baseband USRP board in the low frequency cutoff response of this board.

- This is a baseband board and there is no external RF carrier modulation on the transmitted signal

- However, the USRP board has a low frequency cutoff; this implies that it does not transmit frequencies below a certain RF frequency, due to internal hardware constraints
- Testing with standard sinusoidal signals, it was noticed that this cutoff is close to $25kHz$ for undistorted signal transmission
- Since the baseband L-PPM and OFDM signals occupy the entire low frequency spectrum, this is an undesirable transmitter characteristic of the

This is the baseband transmitter used for all the optical experiments as well. Therefore, in order to overcome this problem of the low frequency cutoff of the USRP board, the transmitted frequency was shifted to the high frequency region, by external modulation by a sinusoidal waveform. This however, signifies that the USRP had an RF carrier at the higher frequency. The transmitted waveform of the L-PPM and the Flip-OFDM are shown here below. This is an important work around for the system, specifically because the USRP showed a low frequency cutoff response.

8.1.3 GnuRadio block

The USRP is interfaced with the GnuRadio software module. The following shows the block diagram of the gnu radio for transmitting and receiving the data

- The noise loading block adds AWGN to the signal based on the desired SNR value
- The input data is stored in a binary format and read by the USRP sink
- The output received signal is read and stored in the same binary file format
- After reading the file, the offline post-processing block is used to demodulate the signal, recover the data and compute the BER for the noise added
- Before analyzing the post processor, there are a few subtle clarifications to be made with respect to the sampling of the OFDM sequence

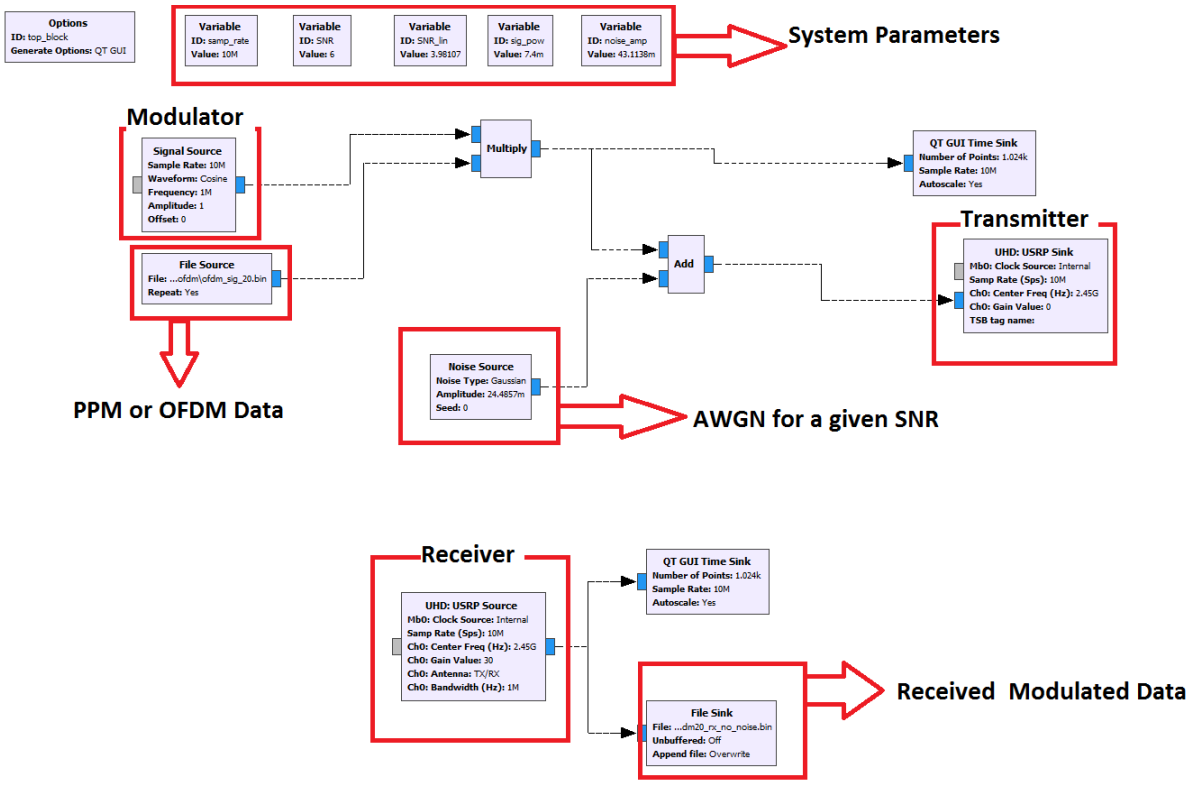

FIGURE 8.2: GnuRadio Block Diagram

8.1.4 Oversampling transmitted data

- The USRP board is a baseband board and hence the modulation is physically done as shown in the block diagram
- The modulation is provided by the signal generator block: multiplied by the cosine
- Modulation of the signal was needed because, the USRP has a low frequency cutoff and directly transmitting the OFDM or PPM signal, results in a signal distortion, hence there is a need to modulate the signal with a cosine waveform generator
- The USRP samples at a rate of $10MSamp/sec$, this means that the data is read at $10MSamp/sec$
- However, the modulator is a cosine of frequency $1MHz$, so the maximum allowable sampling rate is $500kSamp/sec$ In order to overcome this, the data stored in the file is repeated(oversampled) by 32 times; i.e, each sample of data is stored as 32 identical entries
- This results in an information rate of $10M/32 = 312.5kSamp/sec$

- The reason this is done is purely because the data rate has to be slowed down as the modulator and the generation of the carrier are done by the same machine: the USRP; in the actual system, using an external MZM, the laser source will be independently fed to the modulator that can modulate the data at the desired sampling rate

8.1.5 Transmitted data

The following section gives the data parameters of the transmitted data

- L-PPM
  - L: 4
  - Bits transmitted: 4096
  - Number of L-PPM symbols: 2048
  - Oversampling factor: 32
  - Number of samples transmitted: $32 * 2048 = 65536$
  - Information rate: $312.5kSamp/sec$
  - Since each PPM symbol represents half a bit (2 bits encoded as 4 PPM symbols), overall useful bit rate: $156.25kbps$
- Flip OFDM
  - Number of OFDM subcarriers: 256
  - Number of OFDM symbols: 20
  - Flip OFDM, so twice the number of OFDM symbols are needed: 40
  - Number of OFDM samples: $40 * 256 = 10240$
  - Oversampling factor: 32
  - Number of OFDM samples transmitted: $32 * 10240 = 327680$
  - Information rate: $312.5kSamp/sec$
  - Out of 256, 95 subcarriers are independently modulated (Hermitian symmetry, guard band and zero DC); so the net useful information rate is: $\frac{95}{256} * 312.5 = 115.97kSamp/sec$

  - Subcarrier modulation: QPSK
  - Overall useful bit rate: $2 * 115.97 = 231.94 kbps$

- In addition, both the L-PPM and the Flip-OFDM signals have a pn-sequence of length 64 for synchronization; this is explained further in the next section
- The data is continuously transmitted and received by the USRP; in order to process this data, a time window of the total transmitted symbols is taken and passed to the offline post processing
  - The time window is 65536 for L-PPM
  - The time window is 327680 for Flip OFDM
- The received samples are the modulated samples itself as the USRP is a baseband transmitter and it simply sends whatever is put at the input; since the modulation is done physically through GNURadio, the demodulation is also done offline

8.1.6 Offline processing

The following gives a brief description of the offline processing block:

- **Carrier Removal**
  - The carrier removal is done by multiplying the received signal by a sinusoid of same frequency followed by low-pass filtering
  - The low pass filter is taken as a standard First Order FIR Filter with 20 taps and normalized cutoff frequency as 0.05π
- **Synchronization**
  - Since an arbitrary chunk of the repeated data is captured, it is important to synchronize the received samples with the start index
  - In addition to the transmitted data stream, a pn-sequence, consisting of only "zeros" and "ones" is transmitted at the beginning of the data; this is used for finding the start index
  - The pn-sequence has the unique property of having a high autocorrelation and a low correlation factor with other arbitrary sequences

  - The pn-sequnce is already known to the receiver and the method of cross correlation with the captured data is used to find the start index

- **Downsampling**
  - Ideally the best sampling point should be chosen to downsample the sequence, using the eye-diagram
  - However, a simplified approach is used for downsampling and the mid point of the time-domain pulse is used as the best sampling point

- **Demodulation and BER**
  - The demodulation and BER analysis for both PPM and Flip OFDM have been elaborated in the previous chapter
  - Once the sequence is synchronized and downsampled, the demodulation is simply done through the written code for the same

8.1.7 Results

The following section elaborates the results of the given experiment.
Figure (8.3) and Figure (8.4) show the output of the transmitted and received sequence after synchronization and before downsampling, for both L-PPM and Flip-OFDM, for different values of electrical SNR.

- The following two plots show the received noisy signal, after the back to back transmission and offline processing
- The successful synchronization at low SNR values demonstrates the validity of the pn-sequence for synchronization

Figure (8.5) shows the BER Vs SNR analysis for the Flip-OFDM modulation, for this setup.

- An equivalent plot for the L-PPM case is not plotted as the PPM is more robust to the RF back-to-back setup and a zero BER is observed for even very low SNR values

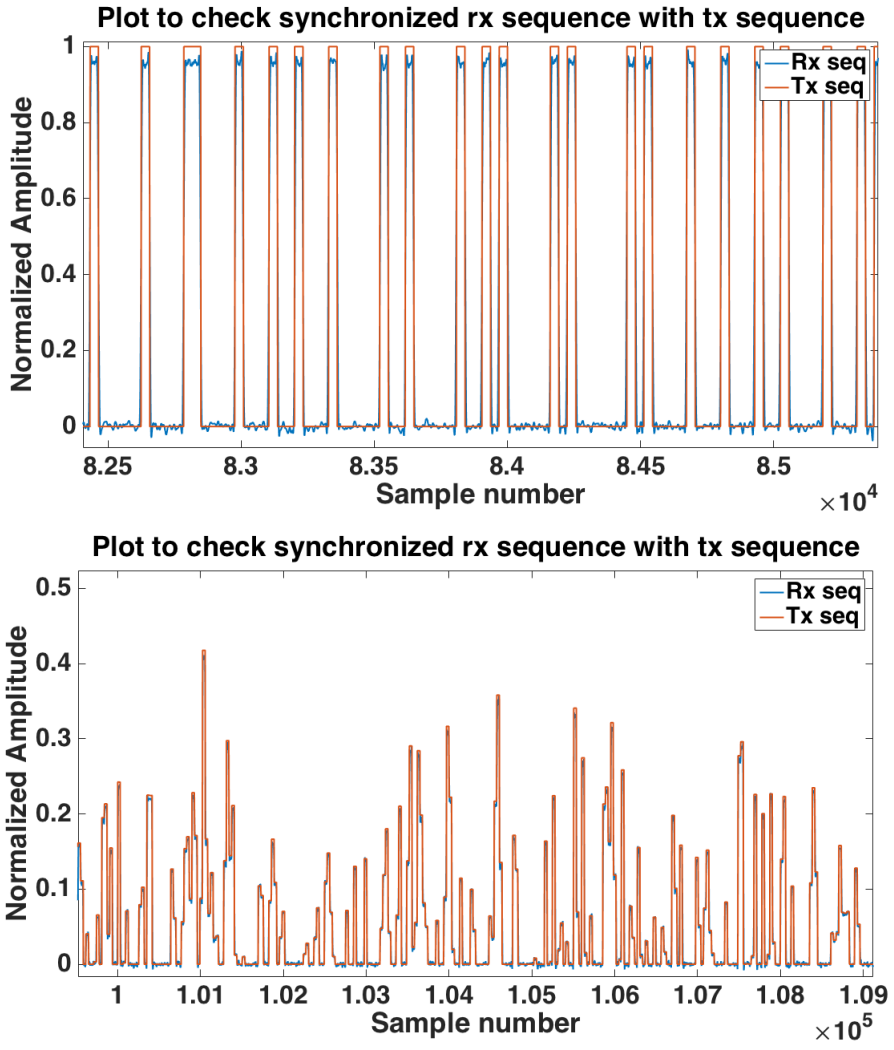

FIGURE 8.3: Received signal: L-PPM and Flip OFDM for an Electrical SNR of 30dB

- The susceptibility of the OFDM modulation to the noise in the system is also clearly seen as a result
- The compromise in the reduced noise tolerance is compensated for increased spectral efficiency and spectral control, as was shown in the previous chapter

8.2 Free Space Optical Communication: Ongoing Experimental Work

The current experimental work is ongoing, as a part of the underwater OFDM project. This section presents a brief overview of this experimental work, the analysis targeted and the future work, moving to the underwater channel.

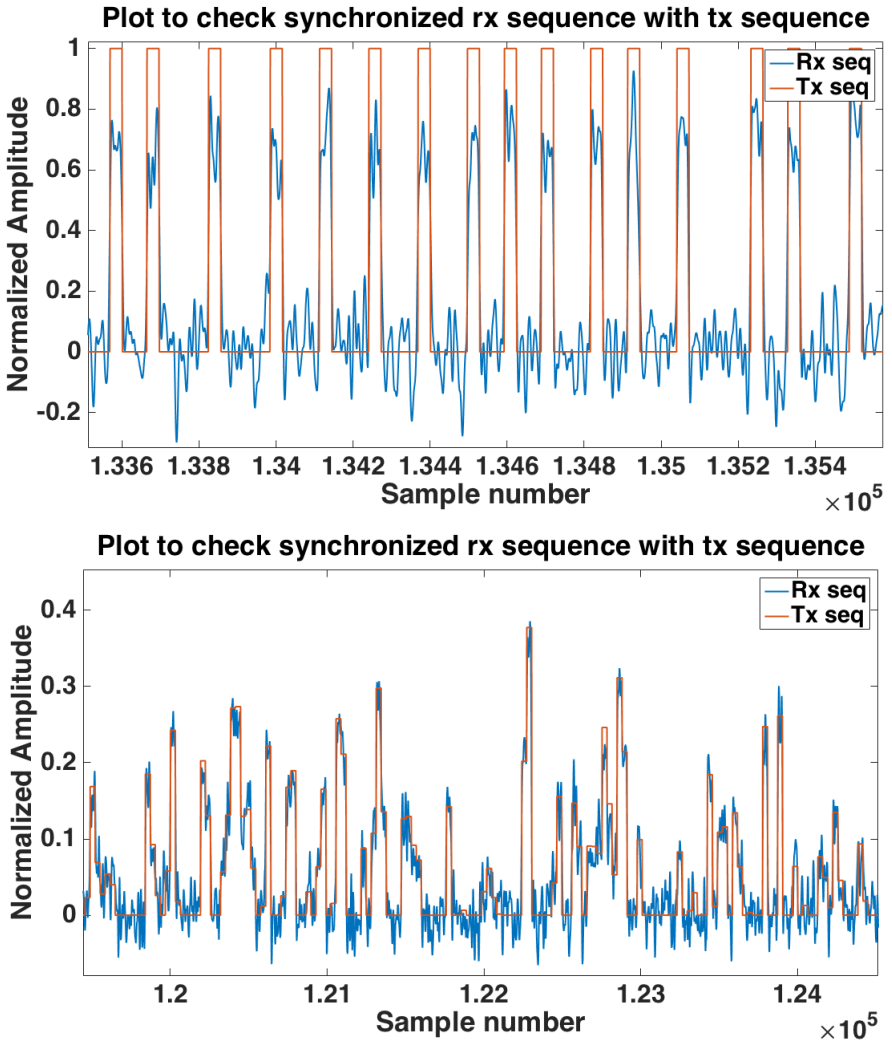

FIGURE 8.4: Received signal: L-PPM and Flip OFDM for an Electrical SNR of $5dB$

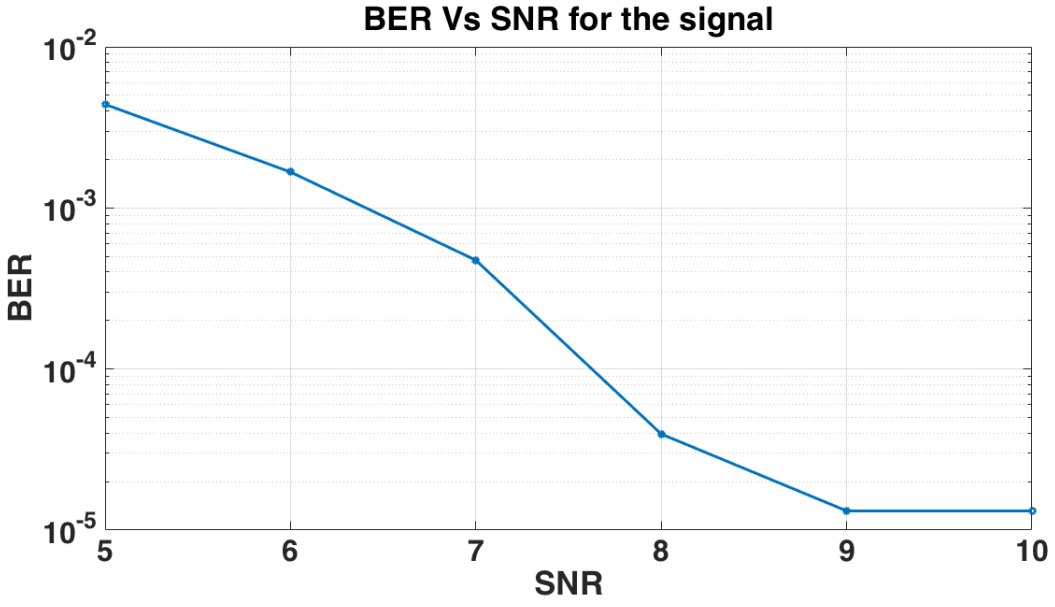

FIGURE 8.5: BER Vs SNR for Flip-OFDM

8.2.1 Experimental block diagram

The Figure (8.7) shows the representative diagram of the experimental setup.

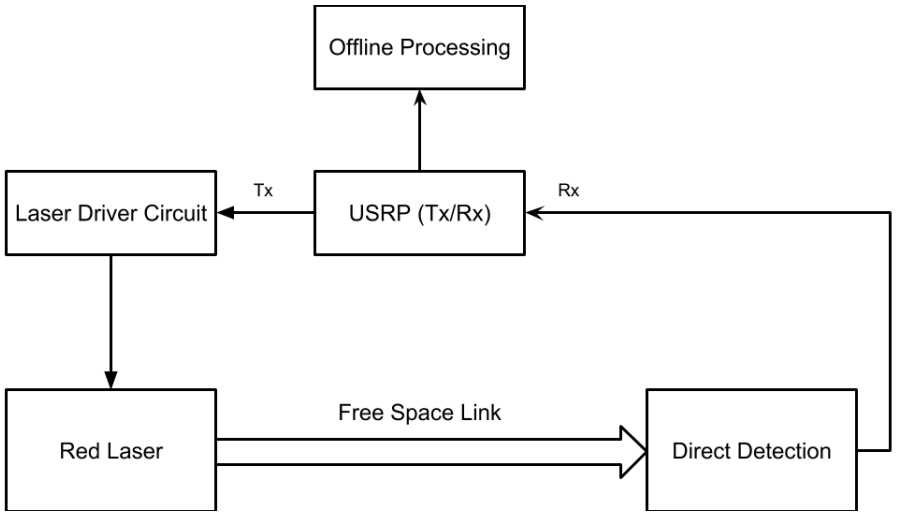

FIGURE 8.6: Overall Block Diagram

- The red laser pointer is present at the SHG frequency, close to $532nm$
- The transmitted waveform is modulated with a carrier, just as was explained in the previous section
- The entire post processing block in the USRP, after receiving the samples is exactly similar to the system described above
- The driver circuitry shown limits the maximum modulating frequency to $50kHz$
  - This means that the maximum carrier modulating frequency is $25kHz$, well within the response of the USRP board
  - The modulation is done at a data rate of $12.5kSamp/sec$, to satisfy Nyquist criterion

8.2.2 Objectives

As a part of this experimental work, the following are the targetted objectves:

- Characterization of the entire circuitry in terms of the transmitted power and received voltage for the back-to-back case

- Theoretical characterization of the free space channel in terms of the scattering and attenuation
- Use of this scattering value to theoretically verify the received power with the actual received power
- Vary the free space distance and characterize the performance as BER Vs Received power

8.2.3 Tasks targeted ahead

Following this setup, the following tasks are planned ahead

- Immerse the whole system in a water channel and repeat the characterization
- Verify the received BER in the water channel as a function of the transmitted power
- Use of OFDM properties to improve the transmission efficiency in the underwater channel

8.3 Conclusions and Future Work

The following presents the different conclusions and tasks ahead for the underwater communication work:

- Through this preliminary analysis, a basic simulation model was presented to analyze the performance of a newly proposed system for the paradigm of underwater communication
- Preliminary experimental work verified the validity of the modulator, demodulator algorithm presented
- A huge part of the task ahead involves the characterization of the underwater channel
  - As stated before, the OFDM modulation presents spectral controlability in terms of preloading and transmitting the subcarriers [19]

  - The inclusion of an accurate underwater channel will further improve the simulation accuracy of the entire system

- Further experimental work with the SHG involves implementation of an optical circuit with the existing RF-optical setup for transmission; however this will require the seed laser at $1064nm$

- Improvement can also been looked at in the modulation to try specific multicarrier formats for highly noisy and unpredictable channels

- The simulation and experimental work has omitted the use of amplifiers; the amplifier model can be used, further adding the nonlinearity to the system to analyze the system performance

- Additional nonlinear precompensation and postcompensation can be looked at to achieve improved performance

- If coherent systems are used, the laser phase noise also begins to affect the transmitted system; analysis of laser phase noise in OFDM [19] shows how the phase noise gets converted to the amplitude noise

Bibliography

[1] Amnon Yariv and Pochi Yeh. *Photonics: optical electronics in modern communications*, volume 6. oxford university press New York, 2007.

[2] Tam N Huynh, Lim Nguyen, and Liam P Barry. Phase noise characterization of sgdbr lasers using phase modulation detection method with delayed self-heterodyne measurements. *Journal of Lightwave Technology*, 31(8):1300–1308, 2013.

[3] Stefano Camatel and Valter Ferrero. Narrow linewidth cw laser phase noise characterization methods for coherent transmission system applications. *Journal of Lightwave Technology*, 26(17):3048–3055, 2008.

[4] N Jeremy Kasdin. Discrete simulation of colored noise and stochastic processes and 1/f/sup/spl alpha//power law noise generation. *Proceedings of the IEEE*, 83(5): 802–827, 1995.

[5] Simon S Haykin et al. *Kalman filtering and neural networks*. Wiley Online Library, 2001.

[6] Lindsay Kleeman. Understanding and applying kalman filtering. In *Proceedings of the Second Workshop on Perceptive Systems, Curtin University of Technology, Perth Western Australia (25-26 January 1996)*, 1996.

[7] Ankita Jain et al. Tracking linear and nonlinear phase noise in 100g qpsk modulated systems using kalman filter. In *Photonic Networks and Devices*, pages JM3A–8. Optical Society of America, 2015.

[8] Luca Barletta, Maurizio Magarini, and Arnaldo Spalvieri. Bridging the gap between kalman filter and wiener filter in carrier phase tracking. *IEEE Photonics Technology Letters*, 25(11):1035–1038, 2013.

[9] Todd Marshall, Bogdan Szafraniec, and Bernd Nebendahl. Kalman filter carrier and polarization-state tracking. *Optics letters*, 35(13):2203–2205, 2010.

[10] Seb J. Savory. *Opt. Express*, 16(2):804–817, Jan 2008. doi: 10.1364/OE.16.000804. URL http://www.opticsexpress.org/abstract.cfm?URI=oe-16-2-804.

[11] S. J. Varughese et al. In *Proc. of NCC 2015*, pages 1–6, Feb 2015. doi: 10.1109/NCC.2015.7084894.

[12] Yuliang Gao et al. *Proc. OFC*, page Th3E.5, 2014. doi: 10.1364/OFC.2014.Th3E.5. URL http://www.opticsinfobase.org/abstract.cfm?URI=OFC-2014-Th3E.5.

[13] Aditya Kakkar, J Rodrigo Navarro, Richard Schatz, Xiaodan Pang, Oskars Ozolins, Hadrien Louchet, Gunnar Jacobsen, and Sergei Popov. Mitigation of eepn in coherent optical systems with low speed digital coherence enhancement. *IEEE PTL*, 27(18):1942–1945, 2015.

[14] Aditya Kakkar, Oskars Ozolins, Jaime Rodrigo Navarro, Xiaodan Pang, Miguel Iglesias Olmedo, Richard Schatz, Hadrien Louchet, Gunnar Jacobsen, and Sergei Popov. Design of coherent optical systems impaired by eepn. In *Optical Fiber Communication Conference*, pages Tu2A–2. Optical Society of America, 2016.

[15] Alan Pak Tao Lau, William Shieh, and Keang-Po Ho. Equalization-enhanced phase noise for 100gb/s transmission with coherent detection. In *OptoElectronics and Communications Conference, 2009. OECC 2009. 14th*, pages 1–2. IEEE, 2009.

[16] Nirmal Fernando, Yi Hong, and Emanuele Viterbo. Flip-ofdm for unipolar communication systems. *IEEE Transactions on Communications*, 60(12):3726–3733, 2012.

[17] G.P. Agrawal. *Nonlinear Fiber Optics*. Optical engineering. Academic Press, 2007. ISBN 9780123695161. URL http://books.google.co.in/books?id=b5S0JqHMoxAC.

[18] Yang Gao, Jianjun Yu, Jiangnan Xiao, Zizheng Cao, Fan Li, and Lin Chen. Direct-detection optical ofdm transmission system with pre-emphasis technique. *Journal of Lightwave Technology*, 29(14):2138–2145, 2011.

[19] Jean Armstrong. Ofdm for optical communications. *Journal of lightwave technology*, 27(3):189–204, 2009.